ATLAS Discovery Potential for the Charged Higgs Boson in $H^\pm \to \tau^\pm \nu_\tau$ Decays

Bjarte Mohn[*]

Department of Physics and Technology, University of Bergen

Martin Flechl[†]

Department of Nuclear and Particle Physics, Uppsala University

Johan Alwall[‡]

Université Catholique de Louvain

(Dated: March 5, 2007)

The ATLAS discovery potential for the hadronic τ decay of a heavy charged Higgs boson, $H^\pm \to \tau^\pm \nu_\tau$, is presented. A new matched production algorithm for the processes $gg \to tbH^\pm$ and $gb \to tH^\pm$ is used allowing to span the investigated mass range from $m_H^\pm < m_t$ up to $m_H^\pm \gg m_t$ with a consistent treatment of the transition region. For the considered charged Higgs boson masses from 165 to 600 GeV, $H^\pm \to \tau^\pm \nu_\tau$ is the most relevant decay channel together with $H^\pm \to tb$. Whereas the latter suffers from large irreducible backgrounds, the τ decay channel offers a decisively cleaner signature. This is the first ATLAS Full Simulation study of the $H^\pm \to \tau^\pm \nu_\tau$ channel. For the background, ATLAS Fast Simulation is used for the investigation of a greater variety of channels than in previous studies, emphasizing the need for new selection cuts with additional discriminating power between signal and background. Such cuts are introduced and it is shown that current limits from direct charged Higgs boson searches can be substantially extended already with a few years of LHC data.

I. INTRODUCTION

Among the most popular extensions of the Standard Model are supersymmetric theories in which the Higgs sector contains five particles, three neutral ones (A^0, H^0, h^0) and two charged ones (H^+, H^-). In the Minimal Supersymmetric Standard Model (MSSM) the most promising decay modes of the charged Higgs boson are fermionic, where $H^\pm \to \tau\nu$ and $H^\pm \to tb$ are the most promising ones. These channels have been studied using ATLAS Fast Simulation (ATLFAST [1]).

As can be seen in current discovery contour plots [2] the transition region where $m_{H^\pm} \approx m_{top}$ is not yet covered by any ATLAS studies. This is related to the fact that at hadron colliders the main contribution to single charged Higgs boson production is through the twin processes $gg \to tbH^\pm$ and $gb \to tH^\pm$ for $m_{H^\pm} > m_{top}$. These are called twin processes since they correspond to two different approximations describing the same basic process. For charged Higgs boson masses above the top quark mass the $2 \to 2$ process is dominant, due to the resummation of potentially large logarithms by the b quark parton density. In this case, the parton shower produces an outgoing b quark. In the region of phase space where the outgoing b quark has large transverse momentum the parton shower does not give a good description of the process, and the full $2 \to 3$ description is needed. However, these two descriptions overlap for small transverse momenta of the b-quark, necessitating a matching procedure to remove resulting double counting as described in Reference [3]. For charged Higgs boson masses below the top quark mass, the

---

[*]Electronic address: bjarte.mohn@ift.uib.no

[†]Electronic address: martin.flechl@tsl.uu.se

[‡]Electronic address: johan.alwall@tsl.uu.se

$2 \rightarrow 3$ process dominates, since it incorporates on-shell top quark pair production with subsequent decay to a charged Higgs boson.

The parameter region where the mass of the charged Higgs boson is similar to the top quark mass is especially complicated since there the two processes are of comparable size. In order to get a reasonable description of this region a matching of the two processes is crucial.

MATCHIG [4] is a new event generator based on the work presented in [3] which matches the two processes by producing negative weight events from an identified double-counting term. In this note we present the first ATLAS Full Simulation study using the MATCHIG generator to cover the transition region. We investigate the $H^{\pm} \rightarrow \tau\nu$ decay mode, previously studied with ATLFAST in [5]. The Feynman diagram in Figure 1 illustrates the signal process. It has the following characteristics:
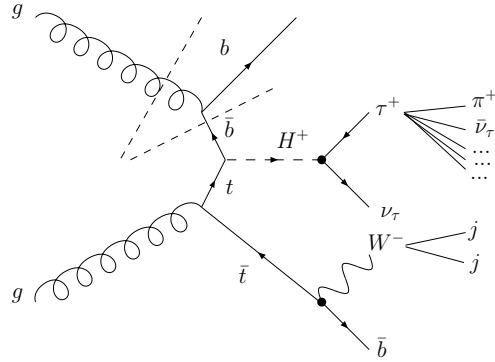

FIG. 1: FEYNMAN DIAGRAM OF THE SIGNAL PROCESS for heavy charged Higgs bosons in the $H^{\pm} \rightarrow \tau\nu_{\tau}$ decay mode. The dashed lines indicate where the factorization between the parton densities and the hard scattering is done, leading either to the $gg \rightarrow tbH^{\pm}$ process or to the $gb \rightarrow tH^{\pm}$ process. They can therefore be viewed as the same process in two different approximations.

- 1 τ lepton decaying hadronically

- significant missing transverse energy (due to the neutrino)

- 2 light jets

- 1 (or 2) b-jets

- 1 W boson (invariant mass $m_{jj} = m_W$)

- 1 top quark (invariant mass $m_{bjj} = m_t$)

- absence of hard, isolated leptons

In the following section we describe how the Monte Carlo samples used for this study were prepared, in terms of event generation, detector simulation and event reconstruction. In Section III a comparative study of this analysis and the previous related work [5] is presented. Improvements to the analysis are discussed in Section IV. In Section V we present the improved results both as discovery contour limits and as limits on the expected signal cross-section times branching ratio. Conclusions are given in Section VII.
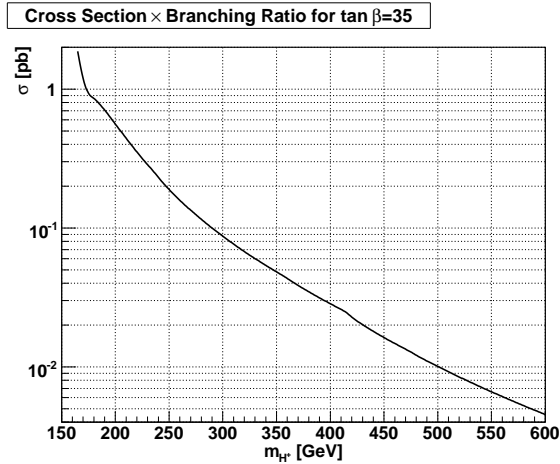
FIG. 2: CROSS SECTION × BRANCHING RATIO for $gb \to tH^{\pm} + gg \to tbH^{\pm}$ with $t \to bjj$ and $H^{\pm} \to \tau^{had}\nu_{\tau}$ for $\tan \beta = 35$.

II. GENERATION, SIMULATION AND RECONSTRUCTION

For both signal and background we use Leading Order (LO) calculations to obtain the total production cross-section values. The signal cross-section ([6, 7]) times relevant branching ratios is shown in Figure 2. The difference between LO and NLO calculations for the signal varies by a factor between 1.3 and 1.6 depending on the mass and $\tan(\beta)$, while for $t\bar{t}$, the main background, the difference between LO (590 pb) and NLO (835 pb [8]) is a factor of approximately 1.4. This leaves our results conservative as we optimize for the significance $\sigma = S/\sqrt{B}$. The leading order signal cross section and branching ratios only depend on $\tan \beta$ and $m_{H^{\pm}}$, assuming a SUSY mass scale large enough to suppress decays to SUSY particles [9].

The detector simulation and reconstruction of signal events was performed using ATLAS Full Simulation while the background (which is several orders of magnitude larger) was simulated using ATLFAST. For a comparison between full and fast simulation performance (see Appendix A), signal events have also been produced using ATLFAST. Different releases of the ATLAS software were used, not only between signal and background, but also between the different steps of signal processing.

A. Signal

The signal as depicted in Figure 1 was generated using MATCHIG as an external process for PYTHIA [10] 6.226 with the ROME underlying event. To ensure the correct treatment of the τ polarisation the τ lepton decays were handled by TAUOLA [11] 2.7 and the final state QED radiation of leptons and hadrons by PHOTOS [12] 2.6. The detector simulation and digitization was performed with ATLAS Software Release 9.0.4 with the ROME-INITIAL detector layout, the reconstruction with Release 11.0.4.

Reconstruction of τ-jets was performed with TAUREC [13] whereas b-jets were tagged using the "CERN-tagger" [14]. The resulting likelihood values were used later in the analysis to select the τ- and b-jets of

the event. A cone algorithm with $\Delta R = 0.4$ was used for the parton jet[1] reconstruction as this matches the ATLFAST jet algorithm. Apart from the above default reconstruction parameters and algorithms were used.

Positive and negative events from MATCHIG were handled separately through all steps of generation, detector simulation and reconstruction. They are finally merged at the analysis level when the distribution of negative events is subtracted from the positive one. The number of events simulated for each charged Higgs boson mass is given in Table I.

As discussed in Appendix A, a comparison between signal analysis with ATLAS Full Simulation and ATLFAST was performed. The ATLFAST signal events were simulated with Athena 9.0.4. For this release, ATLFAST has not been validated and the results should thus be interpreted bearing this in mind.

TABLE I: SIMULATED SIGNAL EVENTS. MATCHIG generates positive and negative events. The production was set to give 10000 matched events, but a small fraction of events were lost during simulation. The number of positive and negative events used in the analysis was thus adjusted in order to restore the correct ratio of positive and negative events as required by the matching procedure. The table shows the final numbers used for this analysis.

Mass [GeV]	Positive events	Negative events	Matched events
165	11432	1595	9837
175	13436	3531	9905
200	13217	3672	9545
300	13735	3973	9762
400	13612	3832	9780
500	13645	3975	9670
600	13877	4181	9696

B. Standard Model Background

The main backgrounds channels for the signal are:

- $t\bar{t}$: The decay mode with one $t \rightarrow bjj$ and the other $t \rightarrow b\tau\nu_\tau$ is the one most similar to the signal signature. However, all decay modes were considered because of the probability of jets to be mistagged as b-jets or τ-jets.

- QCD: Although no hard τ or large p_T^{miss} is present in QCD events, this background has to be considered because of its very high cross section.

- $W +$ jets: There is no top quark present in the event, but it is possible that a W+jet or a multi-jet combination is mistaken for a top quark. W + up to 5 jets was studied. W+1 jet was simulated with all possible W decays, while channels with 2 - 5 extra jets were only simulated with W decays to τ, μ and e.

- Wtb: The final state is similar to $t\bar{t}$, but here one of the two Ws was forced to decay to $\tau\nu$ and the other one into jets.

---

[1] The term "parton jet" is used to distinguish jets initiated by a quark or a gluon from hadronic τ-jets which are initiated by a τ lepton.

Additionally, $Z +$ jets was investigated and found to be negligible. The $t\bar{t}$, QCD and $W + 1$ jet backgrounds were generated with PYTHIA 6.203, simulated with ATLFAST from ATHENA 7.0.3 and has DC1 underlying event. The other $W +$ jets samples include underlying event with Jimmy and were produced with AlpGen [15] by the ATLAS SUSY Working Group using ATHENA (for details, see [16]). The Wtb sample was generated using TopRex [17] with ATHENA release 10. No underlying event except Pythia default was used. The number of simulated events and the cross section is shown for each background channel in Tables II & III.

TABLE II: SAMPLES USED FOR BACKGROUND STUDIES ($t\bar{t}$, QCD, W+1 jet). 'Events' is the number of simulated events. m is the invariant mass of the particles produced in the collision, which is equal to the center-of-mass energy of the colliding partons. p_T refers to the transverse momentum of the W and the additional jet in the rest frame of the hard interaction. All decay modes were simulated. The cross sections σ for the LHC (pp-collisions at a center-of-mass energy of 14 TeV) are given.

$t\bar{t}$			QCD			W+1 jet		
p_T	Events	σ / fb	m / GeV	Events	σ / fb	p_T / GeV	Events	σ / fb
			$20-50$	$4 \cdot 10^7$	$1.22 \cdot 10^{11}$	$10-75$	$2 \cdot 10^7$	$8.15 \cdot 10^7$
			$50-100$	$4 \cdot 10^7$	$4.12 \cdot 10^{11}$	$75-150$	$1 \cdot 10^7$	$3.26 \cdot 10^6$
			$100-200$	$4 \cdot 10^7$	$1.91 \cdot 10^{11}$	$150-200$	$1 \cdot 10^7$	$2.84 \cdot 10^5$
			$200-300$	$4 \cdot 10^7$	$4.80 \cdot 10^{10}$	$200-300$	$1 \cdot 10^7$	$1.21 \cdot 10^5$
all	$2 \cdot 10^7$	$5.9 \cdot 10^5$	$300-400$	$9 \cdot 10^7$	$1.89 \cdot 10^{10}$	$300-400$	$1 \cdot 10^7$	$2.10 \cdot 10^4$
			$400-500$	$3 \cdot 10^7$	$9.22 \cdot 10^9$	$400-500$	$3 \cdot 10^7$	$5.37 \cdot 10^3$
			$500-600$	$4 \cdot 10^7$	$5.14 \cdot 10^9$	$500-600$	$1 \cdot 10^7$	$1.73 \cdot 10^3$
			$600-1000$	$4 \cdot 10^7$	$7.46 \cdot 10^9$	$600-1000$	$1 \cdot 10^7$	$1.11 \cdot 10^3$
			$1000-10000$	$4 \cdot 10^7$	$3.14 \cdot 10^9$	$1000-10000$	$1 \cdot 10^7$	$6.84 \cdot 10^1$

TABLE III: SAMPLES USED FOR BACKGROUND STUDIES (Wtb, W+$\geq$2 jets). The decay of the single-top (Wtb) events was forced such that one W decayed to $\tau\nu$ the other one into jets. All the W+$\geq$2 jets events were simulated with leptonic W decay including all hadronic τ decay modes.

Wtb			W+$\geq$2 jets		
p_T	Events	σ / fb	jets	Events	σ / fb
			W+2jets	$1.41 \cdot 10^7$	$9.4 \cdot 10^5$
all	$1 \cdot 10^7$	$5.9 \cdot 10^5$	W+3jets	$2.71 \cdot 10^6$	$1.8 \cdot 10^5$
			W+4jets	$5.04 \cdot 10^5$	$3.4 \cdot 10^4$
			W+5jets	$1.31 \cdot 10^5$	$8.7 \cdot 10^3$

Because of the high suppression of the QCD events by the selection cuts at least 10^{12} QCD events are required to obtain the very low efficiency of this channel accurately enough. Since the LHC cross section of these processes is very high, this background cannot be neglected although it is largely suppressed and it is crucial to determine its low efficiency very accurately. Even with ATLFAST such a large number of simulated events is not feasible. For this reason a special jet weighting technique was used as illustrated in Table IV. This technique is only used for the QCD events and increases the effective QCD sample size by 3 to 4 orders of magnitude.

TABLE IV: THE JET WEIGHTING TECHNIQUE. All combinations of jets in which one jet is tagged as τ-jet and at least one as b-jet are created and a weight is assigned to each combination, reflecting the probability of this outcome of the jet-tagging during reconstruction. For example, if the truth information lists jet 2 as a b-jet, then $P_{1,II}$ is the b-tagging efficiency, and $P_{2,II}$ the probability that a b-jet is mistagged as τ-jet. All results are then scaled according to the number of simulated events and the cross sections. For an additional example of the use of this technique see Reference [18].

	Jet 1	Jet 2	Jet 3	Jet 4	Weight
Combination 1	$P_{1,I}(\tau|j_1)$	$P_{1,II}(b|j_2)$	-	-	$P_{1,I} \cdot P_{1,II}$
Combination 2	-	$P_{2,II}(\tau|j_2)$	-	$P_{2,IV}(\tau|j_4)$	$P_{2,II} \cdot P_{2,IV}$
Combination 3	$P_{3,I}(b|j_1)$	-	$P_{3,III}(\tau|j_3)$	$P_{3,IV}(b|j_2)$	$P_{3,I} \cdot P_{3,III} \cdot P_{3,IV}$
$\vdots$	$\vdots$	$\vdots$	$\vdots$	$\vdots$	$\vdots$

III.   STANDARD ANALYSIS

To analyze the signal the EVENTVIEW [19] tool was used. The code takes the overlap between different containers of reconstructed physics object candidates within ATHENA into account, by checking that the objects to be inserted are not overlapping in space ($\Delta R < 0.4$) with the ones already inserted. After inserting isolated electrons and muons, the highest priority was given to τ-jets, and the reconstructed τ-candidates passing the cut on the likelihood value calculated by TAUREC were inserterted. After this the b-jets passing the likelihood cut were inserted in case of no overlap in space with the already inserted τ-jet. Finally the light jets were inserted. Once the containers were sorted the EVENTVIEW code looped over each event calculating the required variables and saving them in a ROOT [20] file.

The background ATLFAST ntuples were analyzed separately and a ROOT file containing the same variables as in the signal file was produced. All background jets were also re-tagged with a new and better parametrisation for τ-jet identification in ATLFAST [13].

The b-tagging efficiency was set to 60% (explicitly for ATLFAST, and via the corresponding likelihood cut 0.8 for Full Simulation), a value expected for ATLAS data-taking at low luminosity. This corresponds to a rejection factor of 10 for c-jets and 100 for light jets. For ATLFAST, a flat τ tagging efficiency can be set (with the exception of a small turn-on curve in the low p_T-range which is not relevant to this study). A value of 45% was used, and for the Full Simulation signal this flat efficiency was achieved by a suitable matrix of τ likelihood cut values in the (η_τ, p_T^τ) plane.

To see the effects of using full simulated instead of fast simulated signal and the new and larger background samples, we first perform an analysis in which the same cuts are applied as in previous studies of this channel [5]. The only exception is that a higher τ-tagging efficiency (45% instead of 30%) was used because it was found to significantly improve the results. By applying this optimum tau tagging efficiency the numbers obtained in the analysis presented in this section can be compared to the final results in Section V more easily.

The selection cuts are described below in the sequence in which they are applied. The histograms showing the distributions are filled only with the events passing the previous cut, unless otherwise stated. Distributions for three signal mass points and, wherever appropriate, for $t\bar{t}$, QCD and W+jets background are shown for each step while Wtb is not shown in the plots because the contribution is found to be negligible already at an early stage of the analysis (compare Table V) .

(a) Preselection of jets

A first selection of events is made by requiring exactly one τ-jet (Figure 3) with $p_T^\tau > 40$ GeV, and at

least three more reconstructed light jets with $p_T > 30$ GeV (Figure 4). At least one of them must be a b-jet (Figure 5), but a veto is applied against two or more hard b-jets with $p_T^b > 50$ GeV and $\eta^b < 2.0$ (Figure 6).
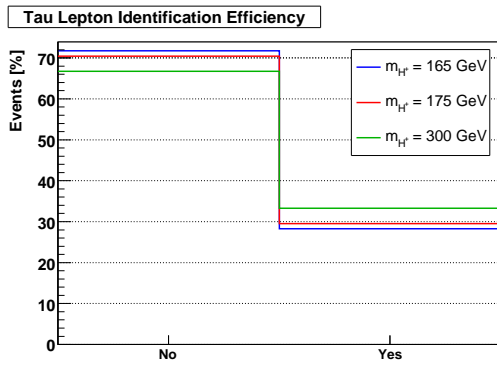

FIG. 3: τ Identification Efficiency. For each event, the probability that the τ from the $H^\pm$ decay is correctly identified is about 30% (τ identification efficiency) for a τ with $|\eta^\tau| < 2.5|$ and $|p_T^\tau > 15$ GeV$|$. This corresponds to a probability of 45% for a τ-jet candidate to be correctly tagged as τ-jet (τ tagging efficiency).
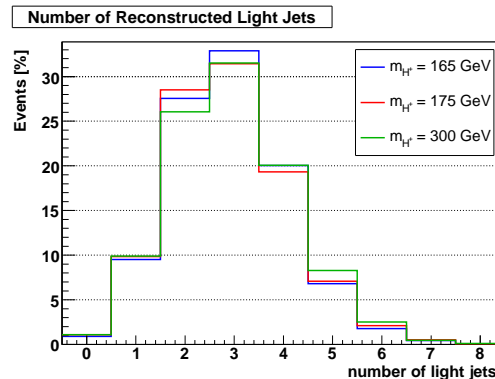
FIG. 4: Number of Reconstructed Light Jets with $p_T > 30$ GeV.

The veto aims towards reducing the $t\bar{t}$ background which has two hard b-jets in most events, and it roughly reduces this background channel contribution by one third. As mentioned, in contrast to previous studies [5], the high tau tagging efficiency of 45% was used because it was found to maximize the signal significance. This tagging efficiency results in a τ identification efficiency of 30% as shown in Figure 3. The loss of roughly two thirds of the signal corresponds to a high suppression of QCD events and of $t\bar{t}$ & W+jets events without decays to a τ. Additionally, a first low cut on the missing transverse momentum requiring at least 40 GeV is applied in order to reduce the large QCD samples early in the analysis.

(b) W Boson and Top Quark Reconstruction

The W boson from the associated top quark decay is reconstructed by first reserving one of the b-jets for the later top quark reconstruction and then retaining all combinations of 2-jets that satisfy $|m_{jj} - m_W$ GeV$| < 25$ (see Figure 7). For ATLFAST m_W was set to true W boson mass of 80.14 GeV, while for the Full Simulation signal it was lowered to 73 GeV because in average the reconstructed W boson mass is found to be about 7 GeV too low, due to a known miscalibration in the software release used. Both for signal and background, the four-momentum of the two-jet system is rescaled by multiplying it by the ratio between true W mass and the mass of the W candidate before the top quark is reconstructed by minimizing the variable $\chi^2 = (m_{jjb} - m_t)^2$ (where m_t is 171 GeV for Full Simulation, and 175 GeV for ATLFAST). It is expected that the performance of this cut will improve for Full Simulation background (and real data) since the resolution of the reconstruced mass is slightly higher in ATLFAST than in Full Simulation (see Appendix A).

If there is more than one b-jet in the event the procedure outlined above is repeated with the next b-jet reserved for the top quark reconstruction. This ensures that all combinations are tested. Finally,
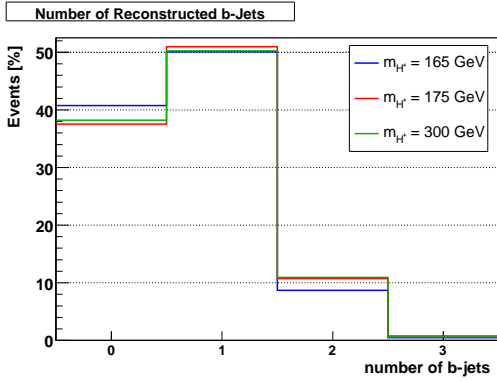
FIG. 5: NUMBER OF RECONSTRUCTED b-JETS WITH $P_T > 30$ GEV. At least one b-jet is required.
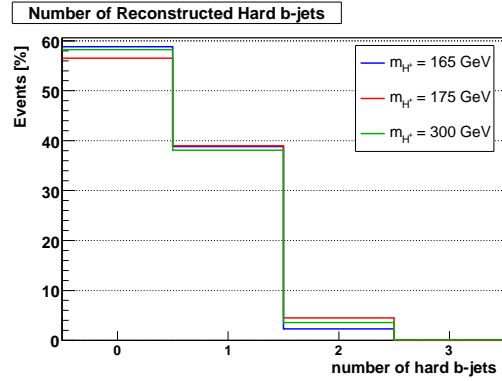

FIG. 6: NUMBER OF HARD b-JETS with $p_T > 50$ GeV in $\eta^b < 2.0$. There is a veto against a second hard b-jet.
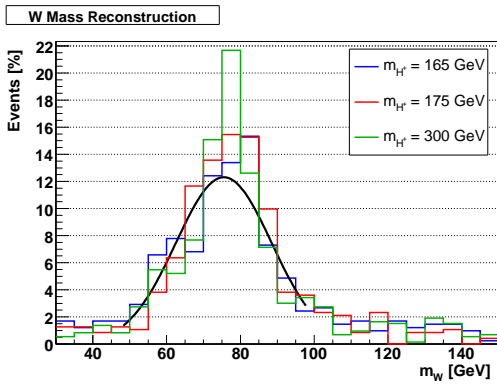

FIG. 7: W BOSON MASS RECONSTRUCTION. The mass of a W boson candidate from one of the systems of two light jets is required to be $|m_{W_{cand}} - 73 \text{ GeV}| < 25$ GeV and is then rescaled to 80.14 GeV. For each event, the best W candidate is shown.
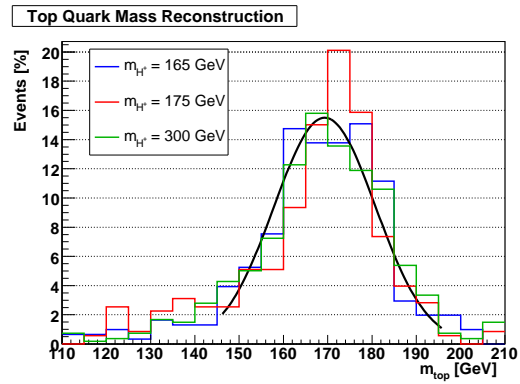

FIG. 8: TOP QUARK MASS RECONSTRUCTION. The mass of a top quark candidate from one of the systems of a W and a b quark is required to be $|m_{t_{cand}} - 171| < 25$. For each event, the best top quark candidate is shown.

the events satisfying $|m_{t_{cand}} - m_t| < 25$ GeV are retained for further analysis (Figure 8).

These are the precuts performed on the large background samples. The events passing these precuts are saved and the rest of the analysis is then done using the significantly smaller event sample.

(c) Transverse Momentum of the Tau Lepton

To further suppress the background, the cut on the transverse momentum of the τ is raised to $p_T^\tau > 100$ GeV. As can be seen in Figure 9, the p_T^τ resolution of the reconstruction is fairly good and most of the very hard τ-jets from a heavy $H^\pm$ decay pass this cut. However, as Figure 10 shows this

cut is very costly for low charged Higgs boson masses: For $m_{H^\pm} = 175$, about 70% of the remaining events are eliminated, for $m_{H^\pm} = 300$ it is still more than 50%. Such a high cut value is aimed towards suppressing the $t\bar{t}$ background, only τ-jets originating from a W with a large p_T boost can satisfy this cut. For a further improvement of the discovery potential alternatives to cut (c) are essential and they are investigated in Section IV.
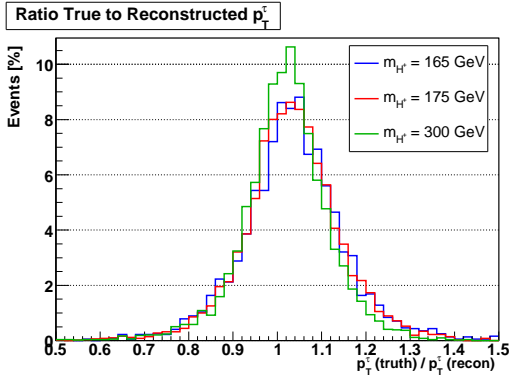

FIG. 9: Ratio of True to Reconstructed Tau Lepton Momentum for all events with a reconstructed τ. Most τ momenta are reconstructed within a $\pm 10\%$ window. Performance is slightly better for a τ from a $H^\pm$ with a higher mass.
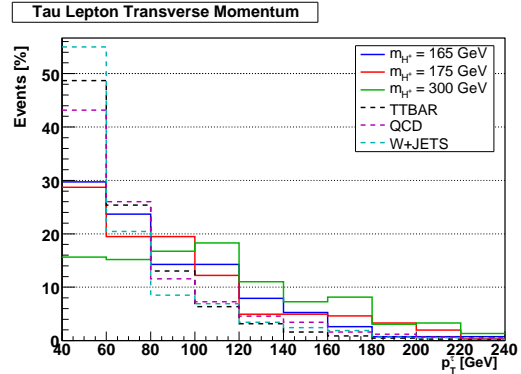

FIG. 10: Transverse Momentum of the Tau Lepton. The p_T^τ is required to be higher than 100 GeV to suppress most of the $t\bar{t}$ background. This, however, also eliminates a large fraction of the signal, in particular for small $m_{H^\pm}$.

(d) Missing Transverse Momentum

A high threshold is applied on the missing transverse momentum, $p_T^{miss} > 100$ GeV. In the QCD events hardly any true p_T^{miss} is present because by definition there are no hard processes involving leptons and thus no hard neutrinos. However, due to the experimental resolution comparatively small tails in the p_T^{miss} distribution exist (see Figure 11) and because of the high cross section of QCD events this still results in a significant contribution to the number of background events.

Again, this cut is not problematic for the high $m_{H^\pm}$ region but in the lower mass region there are hardly any neutrinos which could carry so much missing momentum (see Figure 12) hence almost three quarters of the remaining $m_{H^\pm} = 165$ GeV events are lost.

(e) Azimuthal Opening Angle $\Delta\phi$

As mentioned above, for the background, only τ-jets originating from a W with a large p_T boost can satisfy the p_T^τ cut. A similar statement holds for the ν_τ and the p_T^{miss} cut. This large boost will result in a small azimuthal opening angle $\Delta\phi$ between the decay products τ and ν_τ (see Figure 13). On the contrary, for the $H^\pm \to \tau\nu_\tau$ signal, the $H^\pm$ requires little or no boost (at least for the higher $m_{H^\pm}$ region) to decay to a τ that satisfies the p_T^τ-cut. Therefore a cut is performed on the opening angle between the p_T^τ and the p_T^{miss}. The absolute value of $\Delta\phi$ is required to be greater than 1 radian.

The transverse mass of the $H^\pm$ is given by

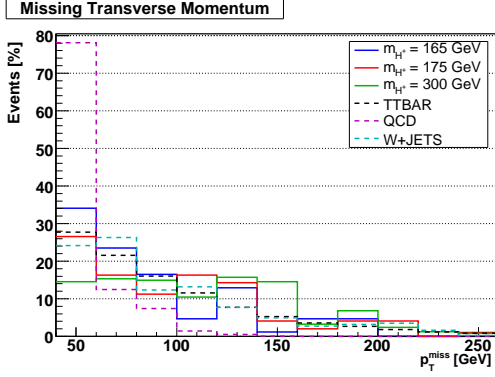$$m_T = \sqrt{2p_T^\tau p_T^{miss} \left[1 - \cos(\Delta\phi)\right]}, \tag{1}$$

FIG. 11: MISSING TRANSVERSE MOMENTUM. A p_T^{miss} threshold of 100 GeV is applied which almost entirely suppresses the QCD background but also eliminates many of the low $m_{H^\pm}$ events.
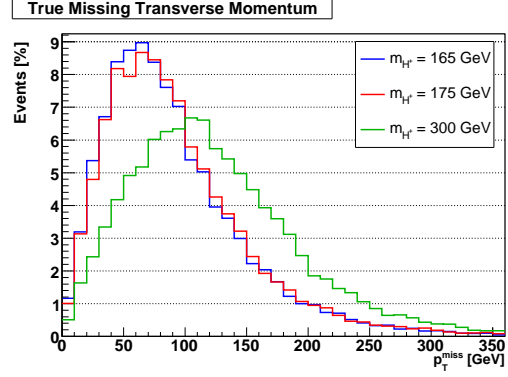

FIG. 12: TRUE MISSING TRANSVERSE MOMENTUM for all signal events. The transverse component of the sum of the four-momenta of all non-interacting particles in the event (in this case, only neutrinos).
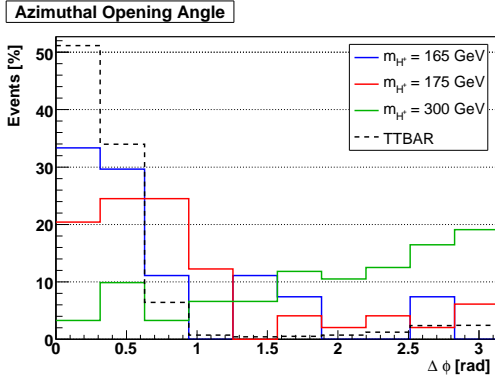

FIG. 13: AZIMUTHAL OPENING ANGLE $\Delta\phi$. The angle between p_T^τ and p_T^{miss} is required to be larger than 1 radian. The distribution has a backward peak not only for $t\bar{t}$ but also for signal events with a small mass $m_{H^\pm}$.
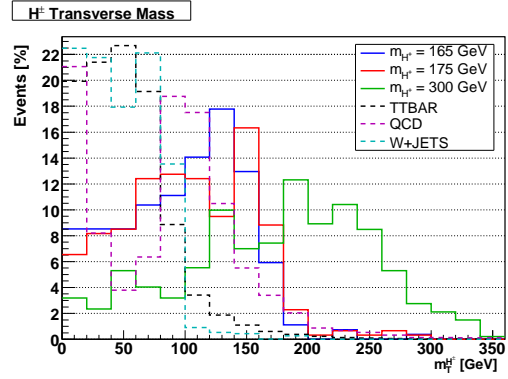

FIG. 14: INVARIANT TRANSVERSE CHARGED HIGGS BOSON MASS. Bound from above by $m_{H^\pm}$, the distribution for $t\bar{t}$ peaks at the W boson mass. No cut is performed.

combining the effects from p_T^τ, p_T^{miss} and $\Delta\phi$. m_T was also considered as a variable for selection cuts because it provides good discrimination between background and signal (Figure 14). If measurement errors are neglected the m_T value is confined from above by the W boson mass for the background, and by the $m_{H^\pm}$ for the signal. However, there is a tail in the background m_T distribution reaching into the signal region due to the limited p_T^{miss} resolution. It was found that better results can be obtained by optimizing these three parameters separately as compared to optimising this one variable comprising the three and thus no cut is performed on m_T.
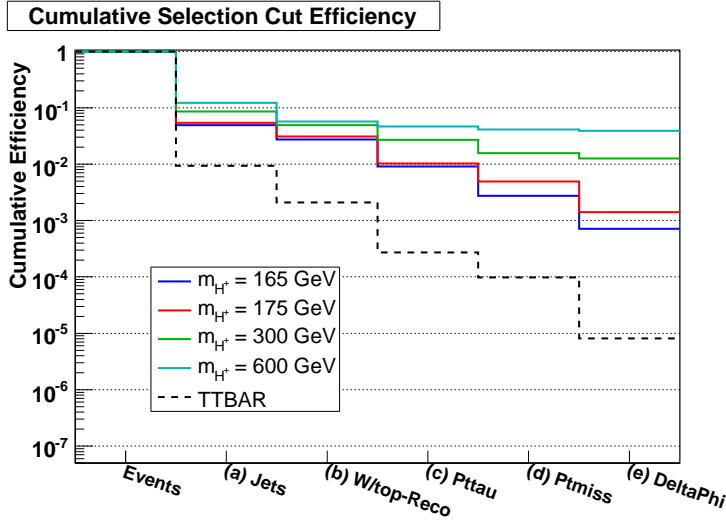
FIG. 15: Cumulative Efficiency of the Selection Cuts for the Signal (Intermediate). The cuts are explained in the text.

Results and Background Estimates

The cumulative signal efficiency is shown in Figure 15. The precuts (a) & (b) affect all mass points in a similar way, whereas the last three cuts result in a much stronger reduction of the signal for low masses as compared to high masses. There is one order of magnitude difference in the signal efficiency between the low and medium masses, and a factor of 50 between the low and the high masses. These values are displayed and compared to the background efficiencies in Table V.

Using the numbers in table V, the significance $\sigma = S/\sqrt{B}$ can be computed, where S and B are respectively the number of signal and background events left after applying all selection cuts. For an integrated luminosity of $30\,\mathrm{fb}^{-1}$ and $\tan\beta = 35$, this results in $\sigma = 3.2, 3.1, 2.6$ and 0.4 for $m_{H^\pm} = 165, 175, 300$ and 600, respectively. The region of the parameter space in which a discovery potential exists is shown in Figure 16.

The new results presented here are different from the previous study [5] based on Atlfast. This is mainly due to our more complete investigation of the background. Only about 17% of the remaining $t\bar{t}$ background is from the $t\bar{t} \rightarrow (W_1 b)(W_2 b)$, $W_1 \rightarrow \tau\nu_\tau$, $W_2 \rightarrow jj$ channel, which was the only one considered in the previous work. The dominating decay modes are now $W_1 \rightarrow \tau\nu_\tau$ and $W_2 \rightarrow l\nu_l$ (33%) and the one where both W decay to $\tau\nu_\tau$ (30%). Furthermore, our investigation of a larger sample of QCD events shows that the contribution of this background channel is not negligible. In fact, it is comparable to the whole background assumed in [5].

TABLE V: CUMULATIVE EFFICIENCIES AND NUMBERS OF SELECTED EVENTS (STANDARD ANALYSIS). Both the cumulative efficiency [/] and the number of events [#] for $\tan\beta = 35$ and an integrated luminosity of $30\,\text{fb}^{-1}$ (corresponding to three years at low luminosity for the ATLAS detector) are shown.

| Cut		Events	Jets (a)	W/t_{rec} (b)	p_T^τ (c)	p_T^{miss} (d)	$\Delta\phi$ (e)
$H_{165}^\pm$	[/]	1	$4.9\,10^{-2}$	$3.3\,10^{-2}$	$9.2\,10^{-3}$	$2.8\,10^{-3}$	$7.1\,10^{-4}$
	[#]	**55940**	**2741**	**1860**	**512**	**154**	**39.8**
$H_{175}^\pm$	[/]	1	$5.4\,10^{-2}$	$4.0\,10^{-2}$	$1.0\,10^{-2}$	$5.0\,10^{-3}$	$1.4\,10^{-3}$
	[#]	**27877**	**1503**	**1103**	**287**	**138**	**39.4**
$H_{300}^\pm$	[/]	1	$8.5\,10^{-2}$	$6.2\,10^{-2}$	$2.7\,10^{-2}$	$1.6\,10^{-2}$	$1.3\,10^{-2}$
	[#]	**2621**	**224**	**162**	**71**	**41**	**33.0**
$H_{600}^\pm$	[/]	1	$1.3\,10^{-1}$	$8.1\,10^{-2}$	$4.4\,10^{-2}$	$4.4\,10^{-2}$	$3.9\,10^{-2}$
	[#]	**136**	**17**	**11**	**6**	**6**	**5.3**
$t\bar{t}$	[/]	1		$2.1\,10^{-3}$	$2.7\,10^{-4}$	$9.8\,10^{-5}$	$8.1\,10^{-6}$
	[#]	**$1.77\cdot10^7$**		**36849**	**4834**	**1741**	**144.2**
QCD	[/]	1		$1.3\,10^{-10}$	$2.7\,10^{-11}$	$5.5\,10^{-13}$	$3.5\,10^{-13}$
	[#]	**$2.45\cdot10^{13}$**		**3227**	**671**	**14**	**8.5**
W+jets	[/]	1		$5.7\,10^{-7}$	$9.6\,10^{-8}$	$3.9\,10^{-8}$	$1.7\,10^{-9}$
	[#]	**$2.56\cdot10^9$**		**1483**	**248**	**101**	**4.5**
Wtb	[/]	1		$6.9\,10^{-5}$	$2.8\,10^{-6}$	$< 10^{-7}$	$< 10^{-7}$
	[#]	**$2.70\cdot10^5$**		**19**	**0.74**	**< 0.1**	**< 0.1**
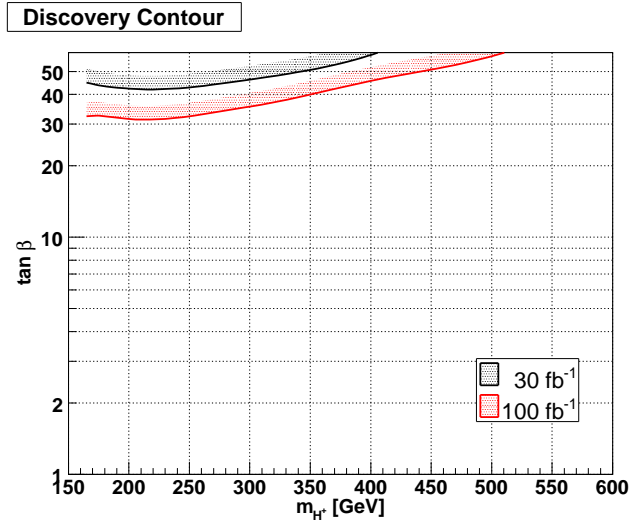
FIG. 16: STANDARD ANALYSIS DISCOVERY CONTOUR. This discovery contour is the result of applying the selection cuts presented in Reference [5]. The regions above the curves are the part of the parameter space in which a 5σ-discovery is feasible. Curves for two different integrated luminosities are shown.

IV. IMPROVED ANALYSIS

In order to improve the results of the analysis described in section III, new selection cuts which provide further discrimination between signal and background are presented and implemented. An important aspect of the analysis is to find cuts which would allow removing or at least loosening of the cuts which lead to a strong reduction of the signal in the low mass region (p_T^τ, p_T^{miss}, $\Delta\phi$) for a selective performance improvement of this part of the parameter space. We have tested a number of other selection variables, and the following three proved to be useful:

- LEPTON VETO[2]: We found that about 53% of the remaining $t\bar{t}$ background is from channels in which at least one W decays to an electron or a muon. The effect of imposing a veto on a hard isolated lepton is to suppress a large fraction of events of these background channels, as well as of channels with a τ which decays leptonically.

- TRANSVERSE MOMENTUM RATIO p_T^τ TO p_T^{-t}: Ratio between the transverse momentum of the τ-jet and the hardest parton-jet which has not been used for the top quark reconstruction[3]. For the $t\bar{t}$ background, such additional jets are expected for most decay modes. For the signal channel, there is only the τ-jet and the three jets used for the top quark reconstruction, and no other hard jets (except for the additional b in the process $gg \to tbH^\pm$, however, this jet is only reconstruced in less than 10% of these events, see below). Because of mistagging (for example of an electron as a jet due to noise in the hadronic calorimeter) and initial/final state radiation, additional reconstructed jets are likely, with increasing probability for a higher $H^\pm$ mass. Since such a higher $H^\pm$ mass in turn implies a harder τ, this cut can be expected to provide an about equally efficient discrimination power between background and signal for all $H^\pm$ masses, unlike the pure p_T^τ cut.

- TAU LEPTON PSEUDORAPIDITY η^τ: The τ-jet η-distribution for the signal is rather central. Additionally, the rejection factor of τ-tagging decreases for larger η, resulting in a large number of fake τ-jets. The cut is thus expected to suppress a significant fraction of all background events in which no true τ-jet is present.

Optimum selection cut values are strongly correlated to the charged Higgs boson mass. Hence for the further analysis the selection cut values are optimized separately for each of the three different mass intervals (in GeV): $m_{H^\pm} < 190$, $190 < m_{H^\pm} < 450$ and $450 < m_{H^\pm}$, refered to as the 'low', 'medium' and 'high' mass ranges. The parameters in question are: Tau Lepton Transverse Momentum (c), Missing Transverse Momentum (d), Azimuthal Opening Angle (e), Tau Lepton Pseudorapidity (g), and Transverse Momentum Ratio (h). The way to apply this to real data in the future would be to first apply the preselection cuts for all events (since they are the same for all mass ranges) and then apply the mass range dependent cut values to the remaining events (a few ten thousand per year at low luminosity).

We also study in detail the more basic quantities used in the analysis, i.e. the τ-jet tagging efficiency (and corresponding rejection) and the required number of tagged b-jets. By adjusting the τ-jet tagging efficiency we simultaneously adjust the rate of background events with fake τ-jets, hence we are able to trade signal for a higher rejection of the reducible background.

---

[2] In this paper the term lepton only refers to isolated e and μ, and not to τ

[3] In the following referred to as 'non-top-jet' meaning 'jet which has neither been used for the top quark reconstruction nor is a τ-jet'.

A.   Implementation

The new cuts were added to the selection chain subsequently in the following order: The Lepton Veto is applied first because it causes almost no loss of the signal and because the value of the cut does not need any adjustment. After applying this cut a more accurate adjustment of the remaining two new cuts is possible. The η^τ cut is applied next and scanned for its optimum, followed by the $p_T^\tau/p_T^{\neg t}$ cut. Finally all cuts are rearranged and grouped (see Section V). The selection cut efficiency plots shown in this chapter correspond to this arrangement, i.e. only those events are considered which have passed the previous cuts in the final sequence.

The cuts on the previously used variables were kept at the values described in Section III during this implementation, with the following exceptions: The cuts on the τ transverse momentum, the missing transverse momentum and the azimuthal opening angle $(p_T^\tau, p_T^{miss}, \Delta\phi)$ which are changed to (65, 120, 1.1) for the low mass region, (80, 135, 1.2) for the medium mass range, and finally (100, 165, 1.3) for the high mass range. Additionally, the precuts were modified by now requiring exactly one b-jet above 30 GeV in the event. All these changes are motivated by scans performed at the end of the analysis.

The impact of the τ-jet tagging was studied by comparing results obtained using different tagging efficiencies. Furthermore, the required number of tagged b-jets and the allowed number of hard b-jets were varied to see the effect on the different charged Higgs boson masses. This was done after adding and optimizing the new cuts. All numbers of events and significances quoted in the following chapters correspond to an integrated luminosity of $30\,\mathrm{fb}^{-1}$ unless stated otherwise. In the context of the new selection cuts (f)-(h) and the b-jet requirements, the significance values stated correspond to the subsequent adding of these cuts, while the efficiencies are given with respect to all the final selection cuts.

(f) Lepton Veto

A veto on an isolated electron or muon with $p_T^{lep} > 7$ GeV is applied. A lepton is considered isolated if the energy deposition in a cone of $0.1 < \delta_R < 0.2$ is smaller than 10 GeV. For the Full Simulation signal, the algorithms used for the reconstruction are Egamma for the electrons, and LowPt MuID, HighPt MuID and MOORE for the muons. The leptons are inserted first. For ATLFAST, a 90% efficiency to identify isolated leptons was assumed. The signal efficiency turns out to be almost insensitive to the p_T^{lep} cut value and thus a low value was chosen in order to suppress as much background as possible.

The Lepton Veto has the expected effect on leptonic $t\bar{t}$ decay channels (see Table VI). When adding the Veto to the analysis performed in section III, about 64% of the background events with leptonic W decays are suppressed, and a small number of events involving a τ decaying to a muon or electron. The backgrounds without true hard leptons and the signal channels remain almost unaffected.

Together with lowering the p_T^τ and p_T^{miss} cuts, this cut increases the significance for $m_{H^\pm} = 165$ GeV from 3.2 to 6.6, for $m_{H^\pm} = 175$ GeV from 3.1 to 3.9, for $m_{H^\pm} = 300$ GeV from 2.6 to 3.5 and from 0.4 to 1.0 for $m_{H^\pm} = 600$ GeV for $\tan\beta = 35$.

(g) τ-jet Pseudorapidity η^τ

A cut on the pseudorapidity η^τ of the tau was added. The optimum cut values were found to be $|\eta^\tau| < 0.9$, $|\eta^\tau| < 1.0$ and $|\eta^\tau| < 1.2$ for the low, medium and high mass region, respectively. As can be seen in Figure 17, this cut is effective because the η^τ distribution of the τ-jets from the $t\bar{t}$ background is rather flat, while the same distribution for the signal has a central peak. This peak, however, diminishes for increasing $m_{H^\pm}$ due to the p_T^τ cut which is relatively softer (compared to the expected p_T^τ spectrum). Thus the optimum cut value for a light charged Higgs boson is smaller than that for a heavier charged Higgs boson. Additionally, a large fraction of the remaining QCD background is suppressed.

The signal efficiency of this cut is almost 100% for the low mass range and about 70% for the medium and high mass range, while the $t\bar{t}$ efficiency is between 17 and 32%, depending on the mass range. For

TABLE VI: BACKGROUND CONTRIBUTION OF THE $t\bar{t}$ DECAY CHANNELS $t\bar{t} \to (bW_1)(bW_2) \to \ldots$ Here 'lepton' refers to electron or muon, 'tau' to tau lepton and 'jet' to parton jet. All numbers refer to the the remaining events after cuts (a)-(e) (left columns), or after the additional Lepton Veto (right columns). For each channel is given: the number of events for an integrated luminosity of $30\,\text{fb}^{-1}$, the contribution to the whole $t\bar{t}$ background in percent, and the selection efficiency.

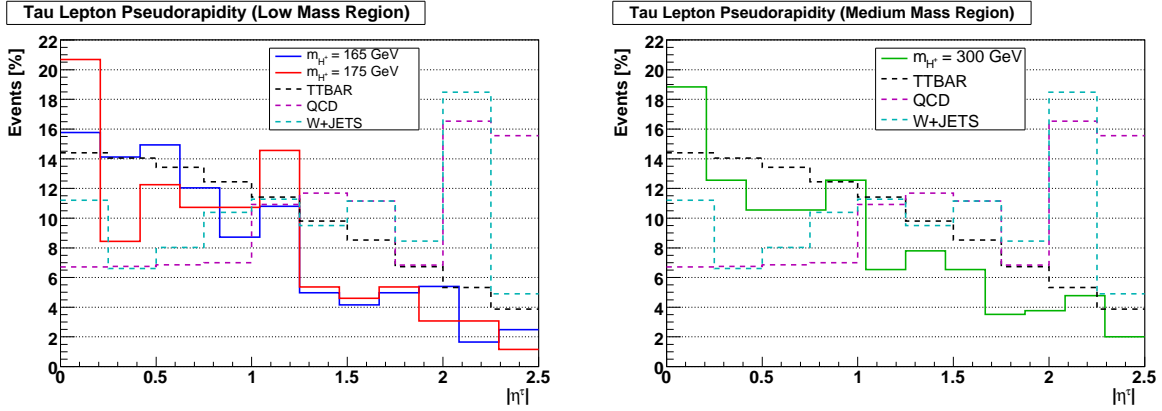| W_1	W_2	EVENTS		PERCENT		EFFICIENCY	
		Precuts	Lepton Veto	Precuts	Lepton Veto	Precuts	Lepton Veto
lepton	lepton	0.9	0.4	0.6	0.5	$2.4\,10^{-7}$	$1.2\,10^{-7}$
lepton	tau	48.2	17.7	33.4	21.4	$1.3\,10^{-5}$	$4.6\,10^{-6}$
lepton	jet	27.6	9.2	19.1	11.1	$1.2\,10^{-6}$	$4.0\,10^{-7}$
jet	tau	24.0	19.5	16.6	23.5	$2.0\,10^{-6}$	$1.6\,10^{-6}$
jet	jet	0.7	0.7	0.5	0.8	$1.9\,10^{-8}$	$1.9\,10^{-8}$
tau	tau	42.8	35.4	29.7	42.7	$4.3\,10^{-5}$	$3.5\,10^{-5}$
ALL		144.2	83.0	100	100	$8.1\,10^{-6}$	$4.7\,10^{-6}$

FIG. 17: τ-JET PSEUDORAPIDITY DISTRIBUTION. Left: low mass range. Right: medium mass range.

$\tan\beta = 35$, this increases the significance for $m_{H^\pm} = 165$ GeV from 6.6 to 12.3, for $m_{H^\pm} = 175$ GeV from 3.9 to 6.5, while for $m_{H^\pm} = 300$ GeV and 600 GeV the significance remains almost unchanged at 3.4 (before: 3.5) and 1.1 (before: 1.0), respectively. For the medium and high mass range, this selection cut only improves the significance together with the following selection cut (h).

(h) p_T Ratio between the τ-jet and the hardest non-top-jet $p_T^\tau/p_T^{\neg t}$

The next step is including the $p_T^\tau/p_T^{\neg t}$ selection cut. This cut is complementary to the Lepton Veto in so far as it affects events with hard additional jets (for example, $t\bar{t}$ decays including $WW \to (jj)(jj)$ and QCD), while the Lepton Veto affects events with leptons (as has been shown, for example $t\bar{t}$ decays via $WW \to (\tau\nu_\tau)(\ell\nu_\ell)$). The $p_T^\tau/p_T^{\neg t}$ distribution for the signal and the $t\bar{t}$ background is shown in Figure 18. The optimum cut $p_T^\tau/p_T^{\neg t}$ value for the low mass region is 6.0, 5.5 for the medium mass range and 5.0 for the high mass range (see Figure 19). The signal efficiency of this additional cut is about 80% for all mass ranges, while the $t\bar{t}$ background efficiency is 15% for the low mass range and about 7% for the medium
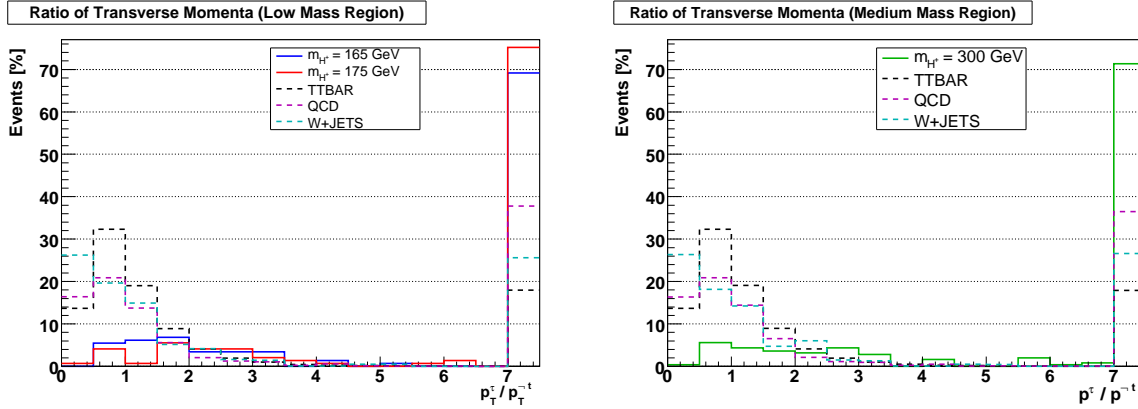
FIG. 18: THE $p_T^\tau/p_T^{\neg t}$ DISTRIBUTION FOR SIGNAL AND BACKGROUND. Left: low mass range. Right: medium mass range. The last bin to the right contains all events with $p_T^\tau/p_T^{\neg t} > 7$. These are mainly the events in which no additional jet is reconstructed and thus $p_T^\tau/p_T^{\neg t} \to \infty$.
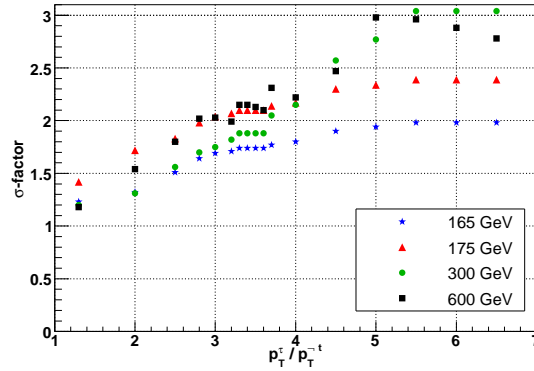

FIG. 19: SIGNIFICANCE: DEPENDENCE ON THE $p_T^\tau/p_T^{\neg t}$ CUT. For four values of $m_{H^\pm}$, the factor by which the significance σ changes (σ-factor) is shown as a function of the value of the cut $p_T^\tau/p_T^{\neg t}$. The best performance is in the medium mass range because there the p_T^τ cut is relatively low compared to the expected p_T^τ spectrum which increases the potential of the p_T ratio cut because of the correlation of these two cuts. This is also true for the high mass range, however, additional jets due to the high activity in these events lead to a slightly worse performance than in the medium mass range.

and high mass range. For $\tan\beta = 35$, this increases the significance for $m_{H^\pm} = 165$ GeV from 12.3 to 24.5, for $m_{H^\pm} = 175$ GeV from 6.5 to 15.8, for $m_{H^\pm} = 300$ GeV from 3.4 to 10.7 and for $m_{H^\pm} = 600$ GeV from 1.1 to 3.1.

As pointed out earlier, the MATCHIG event generator was used in order to match the process descriptions $gg \to tbH^\pm$ and $gb \to tH^\pm$. The procedure used leads to a matched description of the associated b-jet in these two processes. However, in the MATCHIG version used, the emission of additional partons as initial state radiation is not matched to NLO processes such as $gb \to H^\pm tg$. Thus the distribution of such jets in phase space depends on the details of the parton showers and is not necessarily appropriate. Recent studies indicate that by not matching gluon jets to NLO processes the number of additional hard

gluon jets is underestimated and that a proper treatment would lead to a degraded performance of this cut. A decrease of significance by 10 to 20%, depending on the charged Higgs boson mass, is thus expected.
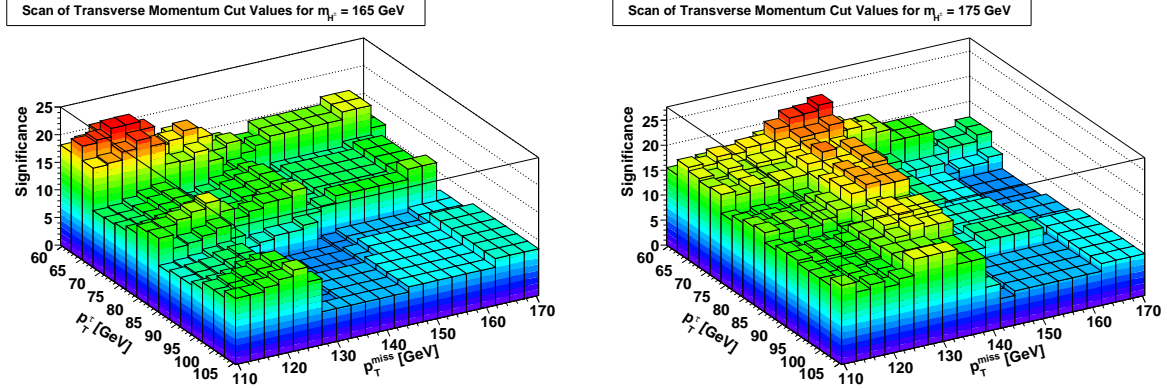
p_T^τ and p_T^{miss} Cut Value Scan

FIG. 20: SCAN OF THE SELECTION CUT VALUES FOR p_T^τ AND p_T^{miss} for $m_{H^\pm} = 165$ GeV (left) and $m_{H^\pm} = 175$ GeV (right) for $\tan\beta = 35$. All other selection cuts are kept constant.
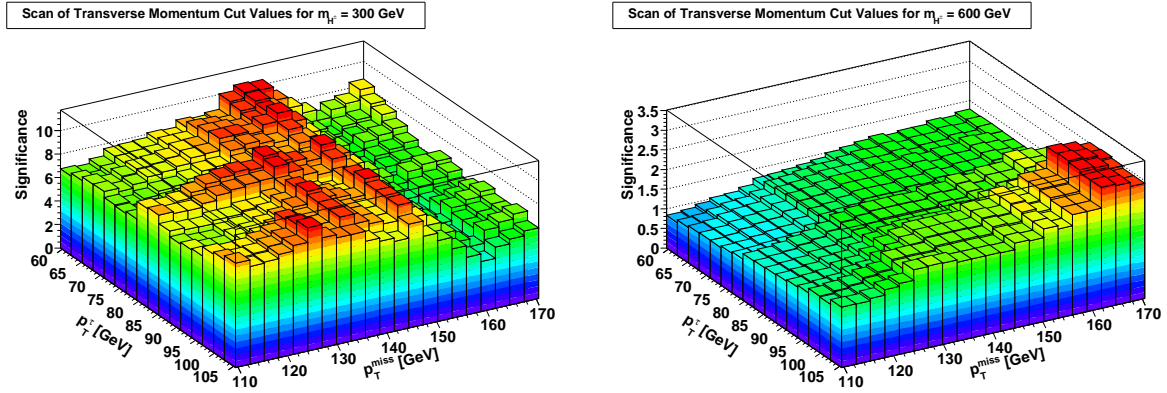

FIG. 21: SCAN OF THE SELECTION CUT VALUES FOR p_T^τ AND p_T^{miss} for $m_{H^\pm} = 300$ GeV (left) and $m_{H^\pm} = 600$ GeV (right) for $\tan\beta = 35$. All other selection cuts are kept constant.

After setting all other selection cut values, the initial choice of the cut values for p_T^τ and p_T^{miss} GeV is confirmed by performing a scan of these values (see Figures 20 and 21). The steep edges in some regions of the plots, in particular for hard cuts at a low charged Higgs boson mass, are due to the small number of remaining events causing large statistical fluctuations. The scans show the need for different selection cut value sets for different mass ranges: For example, the optimum cut value for p_T^τ differs by almost a factor of two.

The dependence of the signal efficiency and the signal significance on the charged Higgs boson mass after applying all cuts is shown in Figure 22.
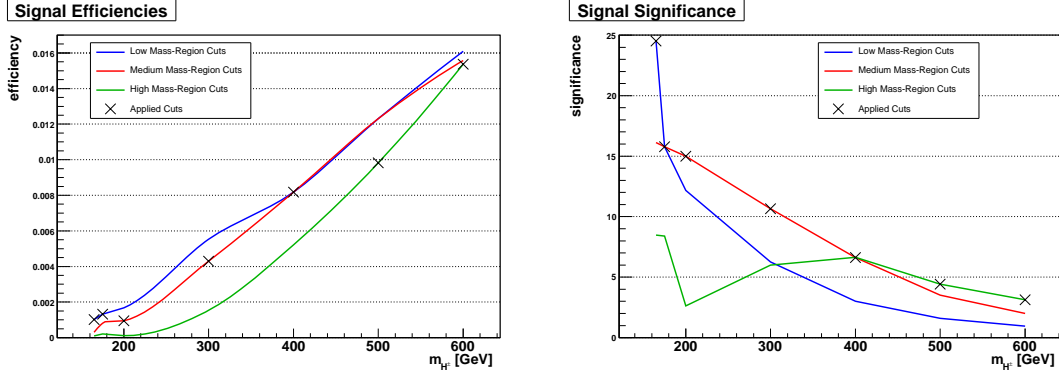

FIG. 22: SIGNAL EFFICIENCY (LEFT) AND SIGNIFICANCE (RIGHT) AS A FUNCTION OF $m_{H^\pm}$. The obtained signal efficiency and significance when applying the different mass range cuts. Only the crosses correspond to working points used in the analysis.

τ-tagging efficiency

As explained in Section III, the highest priority of the reconstruction is given to the τ-jets. A higher efficiency for tagging a τ-jet leads to a lower rejection of other jets. Hence, by varying the likelihood cut on the reconstructed τ-jet candidates it is possible to trade a lower efficiency for the signal against a higher rejection against fake τ-jets.
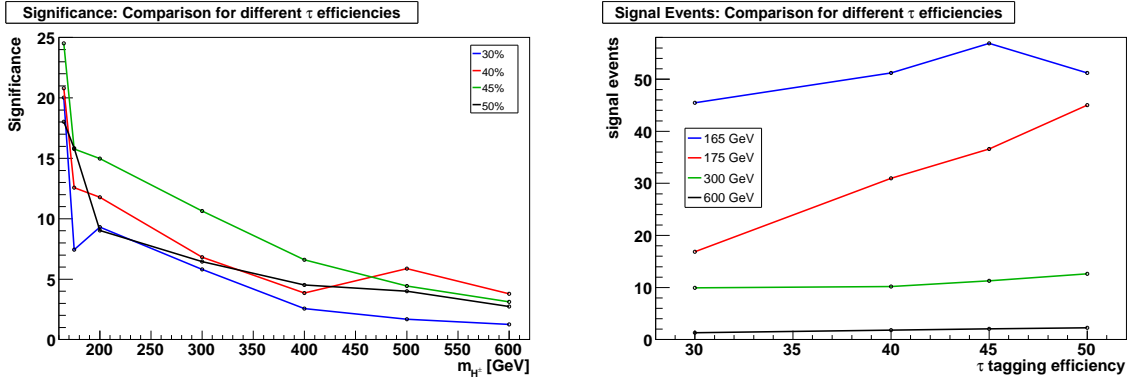

FIG. 23: τ-TAGGING EFFICIENCY STUDIES. Left: signal efficiency as a function of the τ-tagging efficiency. Right: number of signal events as a function of the τ-tagging efficiency for $\tan\beta = 35$ and an integrated luminosity of $30\,\mathrm{fb}^{-1}$.

Figure 23 shows the dependency on the τ-tagging efficiency for both the signal significance and the number of expected signal events. For the low and medium mass range, an efficiency of about 45% is where the optimum performance lies, i.e. the working point where the number of expected signal

events is high and the optimum discovery potential can be obtained. A different working point would degrade the results. This is in agreement with the composition of the background, since when running at 45% the main contributions to the background are $t\bar{t}$ decay modes with real τ-jets. Lowering the efficiency hence results in less background and signal events, but the rate at which they respectively decrease is different. This is related to the fact that a significant contribution to the background comes from $t\bar{t}$ with two real τ-jets in the event, see Table VI. These events have twice the probability for surviving a lower efficiency than the signal, and hence the net result is a degradation of the signal significance. A higher τ-tagging efficiency results not only in more signal events but also more background as the fake rate from both QCD and $t\bar{t}$ increases. Given the large cross-sections of the background this increased fake rate would be larger than the extra signal events, and correspondingly the signal significance would decrease. For the high mass range, slightly higher significancies could be obtained with a τ-tagging efficiency of 40% compared to the 45% used in this study for all mass ranges.

Required number of tagged b-jets

In view of the matched charged Higgs boson production description in the event generator MATCHIG, it is of interest to study the impact of different b-tagging requirements. This is of particular interest since the relative importance of the two contributing production mechanisms is different for different charged Higgs boson masses, see Figure 24.

Despite the fact that 2/3 of the $m_{H^\pm} = 165$ GeV signal is produced through the $2 \to 3$ process, the number of detected b-jets is similar to the other mass points, as shown in Figure 5. Figure 25 shows the contribution from the different production processes to the events with 0, 1 or 2 reconstructed b-jets for $m_{H^\pm} = 165$ GeV. For most of the $2 \to 3$ events, the additional b-jet is not identified as b-jet which can be understood from the distribution of the associated b-jet in the (η, p_T) plane. Jets with $|\eta| > 2.5$ are outside the range of the b-jet tagging algorithm and are hence invisible. In addition we require $P_T > 30$ GeV and together these constraints give rise to a 85% loss (see Figure 26) already before any b-tagging algorithm can be applied.
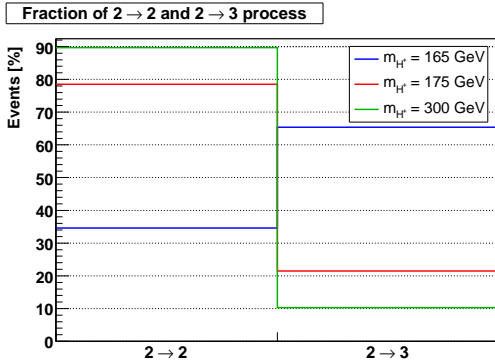

FIG. 24: FRACTIONS OF $H^\pm$ PRODUCTION PROCESSES CONTRIBUTING AT DIFFERENT $m_{H^\pm}$.
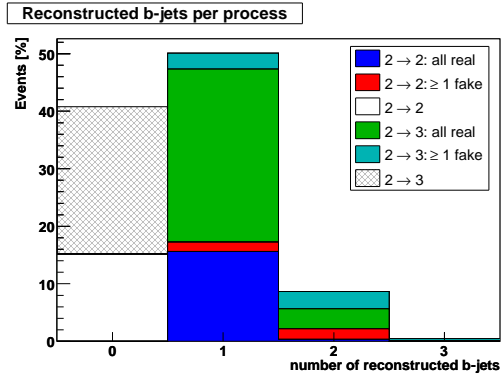
FIG. 25: NUMBER OF RECONSTRUCTED b-JETS PER PROCESS for all events, $m_{H^\pm} = 165$ GeV.

Different requirements for the number of reconstructed b-jets and hard b-jets were tested. b-jets with pseudorapidity $|\eta^b| < 2.0$ and transverse momentum $p_T > 50$ GeV are considered "hard". This definition is motivated by the fact that in $t\bar{t}$ events there are two potentially hard b-jets. The following list shows the different requirements considered:

FIG. 26: (η,p_T)-DISTRIBUTION OF THE ADDITIONAL b-JET in the $2 \rightarrow 3$ process for $m_{H^\pm} = 165$ GeV. The shaded region shows what is visible to the analysis, and only $\sim 1/8$ of the events are found here.
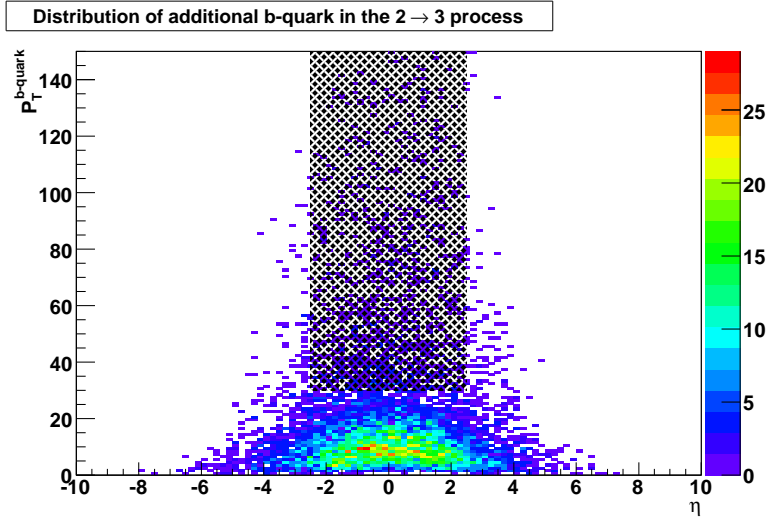
- • $= 1$ b-jet

- • ≥ 1 hard b-jets

- • $= 1$ hard b-jet

- • ≥ 1 b-jet, ≤ 1 hard b-jet (used in Reference [5] and Section III)

- • ≥ 1 b-jet

Figure 27 shows the impact on the signal significance of modifying the precuts to test the different b-jet selections. The differences are small with the exception of the requirement of the presence of exactly one reconstructed b-jet in the event. These leads to the following performance changes with respect to requiring at least one b-jet and at most one hard b-jet: For the low mass range, the number of signal events for $m_{H^\pm} = 165$ GeV is reduced from 63 to 57 (a 9% reduction) while the $t\bar{t}$ background is reduced from 9.6 events to 5.4 events (a 56% reduction). For the medium mass range a comparable performance is achieved, while the high mass range performance is not very sensitive with respect to b-tagging requirements. Hence it is concluded that requiring only one tagged b-jet is the best choice for improving the discovery potential. This requirement is used for the further analysis.

V.   RESULTS

To compare the results obtained in Section IV to the ones obtained in Section III, the selection cuts were rearranged such that the Lepton Veto is now part of the precuts, and the τ-related cuts (η^τ, $p_T^\tau/p_T^{\neg t}$ and p_T^τ, in this order) constitute one group of cuts. The requirement of exactly one tagged b-jet replaces the old cut on having at least one b-jet and at most one hard b-jet. The cumulative efficiency of each group of the selection cut chain is shown in Figure 28. By means of introducing new selection cuts and using three different sets of cut values, the signal efficiencies for the low mass region hardly change while
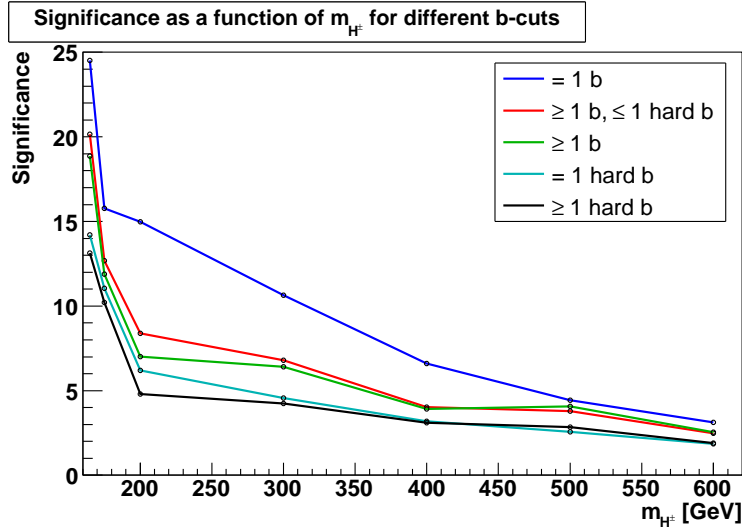
FIG. 27: *b*-TAGGING EFFICIENCY STUDIES. Signal efficiency as function of required *b*-tags for $\tan\beta = 35$ and an integrated luminosity of $30\,\mathrm{fb}^{-1}$. A *b*-jet is considered hard if $p_T^{b-jet} > 50$ GeV and $|\eta^b| < 2.0$. The number of events with two hard *b*-jets after all selection cuts is low, leading to two pairs of curves (for $\geq 1b$ with or without allowing two or more hard *b*-jets, and requiring 1 hard *b*-jets with or without allowing additional hard *b*-jets).
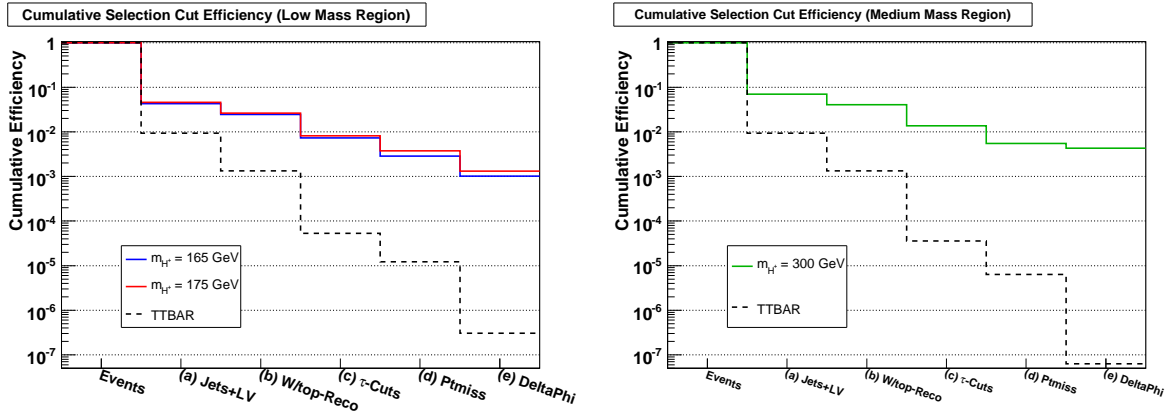
FIG. 28: CUMULATIVE EFFICIENCY OF THE SELECTION CUTS FOR THE SIGNAL. The cuts are explained in the text.

the background rejection improves by a factor of 30. For the medium and high mass ranges, the number of expected background events decreases by 2-3 orders of magnitude, while the signal efficiency decreases only by a factor of 3 or less. The selection cut flow is illustrated in more detail in Table VII. The event selection cuts are summarized below (the brackets refer to {low mass range, medium mass range, high mass range}):

- Jets+LV:

    exactly one τ-jet with $p_T^\tau > 40$ GeV, $p_T^{miss} > 40$ GeV, at least three parton jets, among those

exactly one b-jet, no isolated lepton with $p_T^{lep} > 7$ GeV.

- W/t_{rec}:

  two jets with $|m_{jj} - m_W| < 25$ GeV, the same two jets plus the b-jet with $|m_{jjb} - m_t| < 25$ GeV.

- τ-Cuts:

  $|\eta^\tau| < \{0.9, 1.0, 1.2\}$, $p_T^\tau/p_T^{-t} > \{6.0, 5.5, 5.0\}$, and $p_T^\tau > \{65, 80, 100\}$.

- $p_T^{miss} > \{120, 135, 165\}$.

- $\Delta\phi > \{1.1, 1.2, 1.3\}$.

TABLE VII: Cumulative Efficiency and Numbers of Selected Events. Both the cumulative efficiency [/] and the number of events [#] for $\tan\beta = 35$ and an integrated luminosity of $30\,\text{fb}^{-1}$ (corresponding to three years at low luminosity for the Atlas detector) are shown.

Cut		Events	Jets+LV (a)	W/t_{rec} (b)	τ-Cuts (c)	p_T^{miss} (d)	$\Delta\phi$ (e)
Low Mass Range Cuts
$H^\pm_{165}$	[/]	1	$4.3\,10^{-2}$	$2.4\,10^{-2}$	$7.3\,10^{-3}$	$2.8\,10^{-3}$	$1.0\,10^{-3}$
	[#]	55940	2400	1370	409	159	56.9
$H^\pm_{175}$	[/]	1	$4.6\,10^{-2}$	$2.6\,10^{-2}$	$8.2\,10^{-3}$	$3.7\,10^{-3}$	$1.3\,10^{-3}$
	[#]	27877	1283	737	228	104	36.6
$t\bar{t}$	[/]	1		$1.3\,10^{-3}$	$5.3\,10^{-5}$	$1.2\,10^{-5}$	$3.0\,10^{-7}$
	[#]	$1.77 \cdot 10^7$		23763	939	216	5.4
Other Bkg [#]		$2.45 \cdot 10^{13}$		3891	165	9	<0.1
Medium Mass Range Cuts
$H^\pm_{200}$	[/]	1	$5.6\,10^{-2}$	$3.2\,10^{-2}$	$8.2\,10^{-3}$	$2.3\,10^{-3}$	$1.0\,10^{-3}$
	[#]	16831	942	531	138	39	15.9
$H^\pm_{300}$	[/]	1	$7.0\,10^{-2}$	$4.1\,10^{-2}$	$1.4\,10^{-2}$	$5.5\,10^{-3}$	$4.3\,10^{-3}$
	[#]	2621	183	107	36	14	11.3
$H^\pm_{400}$	[/]	1	$8.2\,10^{-2}$	$4.0\,10^{-2}$	$1.4\,10^{-2}$	$9.1\,10^{-3}$	$8.2\,10^{-3}$
	[#]	855	70	36	12	8	7.0
$t\bar{t}$	[/]	1		$1.3\,10^{-3}$	$3.6\,10^{-5}$	$6.4\,10^{-6}$	$6.3\,10^{-8}$
	[#]	$1.77 \cdot 10^7$		23763	632	113	1.1
Other Bkg [#]		$2.45 \cdot 10^{13}$		3891	130	7	<0.1
High Mass Range Cuts
$H^\pm_{500}$	[/]	1	$8.6\,10^{-2}$	$4.1\,10^{-2}$	$1.9\,10^{-2}$	$1.0\,10^{-2}$	$1.0\,10^{-2}$
	[#]	302	26	12	6	3.1	3.0
$H^\pm_{600}$	[/]	1	$1.0\,10^{-1}$	$4.8\,10^{-2}$	$2.3\,10^{-2}$	$1.6\,10^{-2}$	$1.5\,10^{-2}$
	[#]	136	14	7	3	2.2	2.1
$t\bar{t}$	[/]	1		$1.3\,10^{-3}$	$2.2\,10^{-5}$	$2.5\,10^{-6}$	$2.5\,10^{-8}$
	[#]	$1.77 \cdot 10^7$		23763	390	45.1	0.4
Other Bkg [#]		$2.45 \cdot 10^{13}$		3891	112	3.0	<0.1

In Table VIII, the composition of the dominating background $t\bar{t}$ is shown for the whole selection cut chain. The main contribution after applying all cuts is the decay channel where both W decay to a τ lepton and a neutrino. This is the case because the final cut on $\Delta\phi$ is applied to an almost flat distribution which is the result of the presence of a second hard neutrino (the same can be observed for the decay channel where one W decays to a τ lepton, and the other to an electron or a muon and a neutrino). For the decay mode closest to the signal signature ($W_1 \rightarrow \tau\nu$, $W_2 \rightarrow jj$), $\Delta\phi$ truely describes the angle between the τ-jet and the neutrino and thus the cut on $\Delta\phi$ suppresses this channel almost entirely following the hard cuts on the transverse momentum of the τ-jet and the neutrino.

TABLE VIII: COMPOSITION OF THE $t\bar{t}$ BACKGROUND. Contributions of the decay channels $t\bar{t} \rightarrow (bW_1)(bW_2) \rightarrow \ldots$ The number of selected events after each cut for $\tan\beta = 35$ and an integrated luminosity of $30\,\mathrm{fb}^{-1}$ are shown.

W_1	W_2	Events	W/t_{rec} (b)	τ-Cuts (c)	p_T^{miss} (d)	$\Delta\phi$ (e)
Low Mass Range Cuts						
lepton	lepton	822000	3	1	0	0.0
lepton	tau	858000	436	18	2	1.1
lepton	jet	8090000	330	11	2	1.6
jet	tau	2690000	22000	869	208	0.9
jet	jet	5160000	303	2	0	0.0
tau	tau	224000	661	38	3	1.8
SUM		17700000	23800	939	216	5.4
Medium Mass Range Cuts						
lepton	lepton	822000	3	0	0	0.0
lepton	tau	858000	436	13	1	0.4
lepton	jet	8090000	330	5	0	0.0
jet	tau	2690000	22000	587	111	0.0
jet	jet	5160000	303	2	0	0.0
tau	tau	224000	661	24	1	0.7
SUM		17700000	23800	632	113	1.1
High Mass Range Cuts						
lepton	lepton	822000	3	0	0	0.0
lepton	tau	858000	436	6	0	0.2
lepton	jet	8090000	330	2	0	0.0
jet	tau	2690000	22000	364	44	0.0
jet	jet	5160000	303	2	0	0.0
tau	tau	224000	661	16	0	0.2
SUM		17700000	23800	390	45	0.4

The resulting discovery contour for the MSSM is displayed in Figure 29. A significant improvement compared to Section III (compare 16) has been achieved for all charged Higgs boson masses considered: For $\tan\beta > 41$, a discovery potential exists for all considered $m_{H^\pm}$ with three years of ATLAS data at low luminosity, and for $\tan\beta > 33$ after collecting data representing an integrated luminosity of $100\,\mathrm{fb}^{-1}$. For $m_{H^\pm} < 160$ GeV a discovery is possible within the first years regardless of $\tan\beta$, and this region extends almost up to the top quark mass in the following years. This can be concluded from the results for the charged Higgs boson masses of 165 and 175 GeV, by extrapolating the obtained signal efficiencies to the region around 160 GeV and taking into account the steep increase of the cross section for these

low masses, see figure 2. This is in good agreement with the results obtained for a light charged Higgs boson [21].
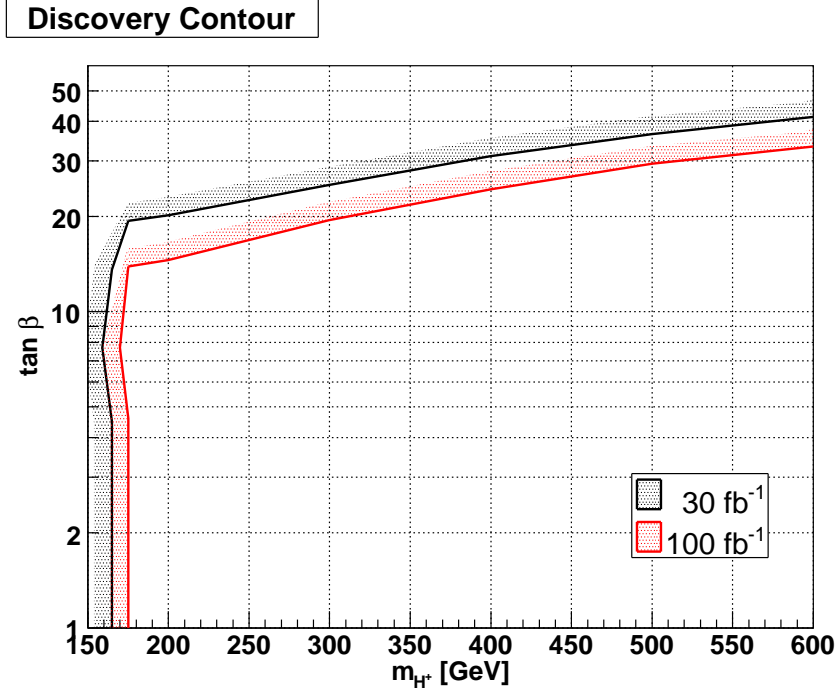

FIG. 29: CHARGED HIGGS BOSON DISCOVERY CONTOUR $m_H^{\pm}$ VS $\tan\beta$ IN THE MSSM. The regions above the curves are the part of the parameter space in which a 5σ-discovery is feasible. Curves for two different integrated luminosities are shown.

A model-independent plot showing the discovery contour as a function of the charged Higgs boson mass and the cross section (including relevant branching ratios) is presented in Figure 30. The sensitivity to a charged Higgs boson discovery increases quickly with the charged Higgs boson mass until about 350 GeV and continues increasing for higher masses, but more slowly. The steep decrease of the cross section with increasing charged Higgs boson mass in the MSSM explains the shape of the discovery contour in Figure 29.

VI.   SYSTEMATIC UNCERTAINTIES

For the investigated channel, the three largest potential sources of systematic effects on the statistical significance are:

- Error of the luminosity measurement: $\Delta\mathcal{L} = \pm 10\%$

- Uncertainty of the $t\bar{t}$ cross section: $\Delta\sigma = \pm 10\%$

- Uncertainty of the τ tagging efficiency: $\Delta\epsilon_{tautag} = \pm 4\%$

For the luminosity measurement, the ultimate aim is to reduce its systematic error to 5% [22]. However, for this investigation the error is conservatively assumed to be 10% considering the experience at hadron
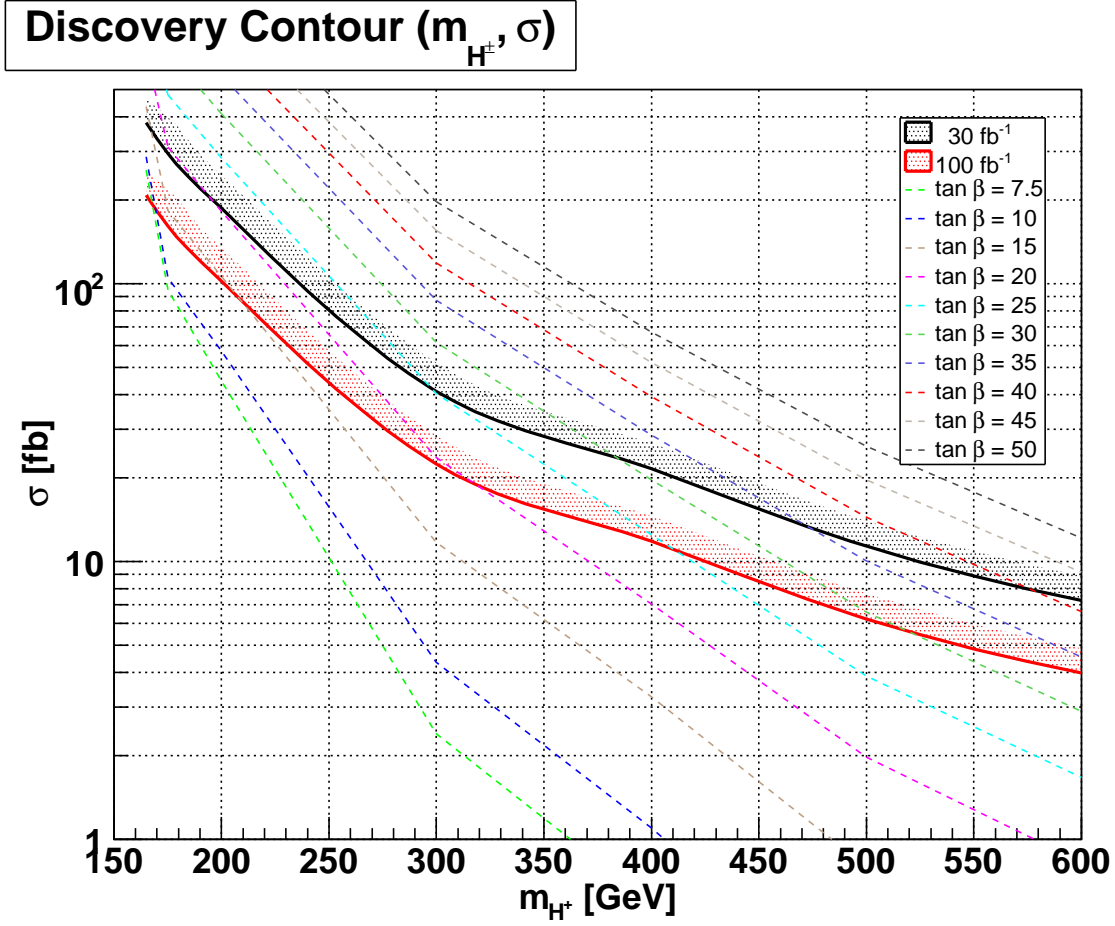
Discovery Contour ($m_{H^\pm}$, σ)

FIG. 30: CHARGED HIGGS BOSON DISCOVERY CONTOUR $m_H^\pm$ VS CROSS SECTION. The regions above the curves indicate cross section values for the processes $gb \to tH^\pm$ and $gg \to tbH^\pm$ with $t \to bjj$ and $H^\pm \to \tau^{had}\nu_\tau$ for which a 5σ-discovery is feasible. Curves for two different integrated luminosities are shown, together with cross sections for different values of $\tan\beta$ in the MSSM. The minimum of the charged Higgs boson production cross section is approximately at $\tan\beta = 7.5$.

colliders and the detector specifications [23]. The uncertainty of the $t\bar{t}$ cross section is taken into account by assuming that this cross section will be known with a precision of 10% from LHC and Tevatron data [22]. Since the τ-tagging is crucial for the results presented, the uncertainty on the τ-tagging efficiency is considered and taken to be 4% [24] following the most pessimistic scenario.

The worst-case significance as a consequence of each systematic uncertainty (σ_{w_i}) is computed, constituting a contribution to the error of the statistical significance given by

$$\Delta\sigma_{sys_i} = \sqrt{\sigma^2 - \sigma_{w_i}^2} \qquad (2)$$

where σ is the statistical significance without taking into account the systematic uncertainties. The total contribution of the systematic effects is given by quadratically summing all contributions:

$$\Delta\sigma_{sys,tot} = \sqrt{\sum \Delta\sigma_{sys_i}^2} \qquad (3)$$

which leads to the final significance

$$\sigma_{final} = \sqrt{\sigma^2 - \Delta\sigma_{sys,tot}^2}. \qquad (4)$$

TABLE IX: INFLUENCE OF SYSTEMATIC UNCERTAINTIES ON THE SIGNIFICANCE. The calculations have been performed for $\tan\beta = 35$ and an integrated luminosity of $30\,\mathrm{fb}^{-1}$.

SYSTEMATIC UNCERTAINTY		CHARGED HIGGS BOSON MASS $m_{H^\pm}$ [GeV]						
		165	175	200	300	400	500	600
$\mathcal{L}$ ($\pm 10\%$)	σ_{w_1}	23.4	15.0	14.3	10.2	6.3	4.2	3.0
	$\Delta\sigma_{sys_1}$	7.4	4.7	4.5	3.2	2.0	1.3	1.0
$\sigma(t\bar{t})$ ($\pm 10\%$)	σ_{w_2}	23.4	15.0	14.3	10.2	6.3	4.2	3.0
	$\Delta\sigma_{sys_2}$	7.4	4.7	4.5	3.2	2.0	1.3	0.9
τ-tagging ($\pm 4\%$)	σ_{w_3}	20.3	13.1	9.7	6.9	4.3	2.6	1.8
	$\Delta\sigma_{sys_3}$	13.8	8.9	11.4	8.1	5.1	3.6	2.6
$\Delta_{sys,tot}$		17.4	11.1	13.1	9.3	5.8	4.1	2.9
σ		24.5	15.8	15.0	10.7	6.6	4.4	3.1
σ_{final}		17.4	11.2	7.3	5.2	3.2	1.7	1.1

The contributions of the uncertainties for each systematic effect, the total systematic uncertainty and the final significance are given in Table IX for all simulated mass points at $\tan\beta = 35$. The systematic uncertainties are heavily dominated by the contributions of the τ-tagging. However, it should be pointed out that all assumptions concerning the sources of potential systematic uncertainties represent a worst-case-scenario and there is hope that they can be reduced in the future. When taking systematic uncertainties into account, the significance decreases by 30 to 60%, depending on the charged Higgs boson mass.

VII. CONCLUSIONS

The ATLAS discovery potential of the charged Higgs boson in the decay $H^\pm \to \tau\nu_\tau$ has been investigated covering the region above $m_{H^\pm} > m_{top}$ and additionally, for the first time the transition region $m_{H^\pm} \approx m_{top}$. The decay channel $H^\pm \to \tau\nu_\tau$ is significant for large $\tan\beta$ and offers a much clearer signal than the other main channel in this mass region, $H^\pm \to tb$, dominating for low $\tan\beta$. In this region, the low branching ratio $H^\pm \to \tau\nu_\tau$, together with the fact that the cross section for $gg \to tbH$ and $gb \to tH$ has its minimum at $\tan\beta \approx \sqrt{\frac{m_{top}}{m_b}} \approx 7.5$, makes the region $\tan\beta < 10$ hard to access.

A matched production for the channels $gg \to tbH$ and $gb \to tH$ was used for a charged Higgs boson mass 165 GeV$\leq m_{H^\pm} \leq$ 600 GeV. The subsequent decays of the top quark and the charged Higgs boson $t \to jjb$ and $H^\pm \to \tau\nu_\tau$ were considered. Following previous studies, a high threshold on p_T^τ and p_T^{miss} was imposed such that for the backgrounds the W boson decay products require a large boost in order to pass the cuts, resulting in a small azimuthal opening angle between the τ lepton and the missing

momentum vector. This is not the case for the signal and the difference between signal and background increases for higher charged Higgs boson masses.

Compared to previous studies a more complete treatment of the background was performed resulting in an increase in the estimated number of remaining background events by more than one order of magnitude. This together with very low selection cut efficiencies for the low mass charged Higgs boson lead to the requirement of more efficient selection cuts in order to improve the discrimination between signal and background. As a first step, the signal selection cuts following the precuts were separately optimized for the low, medium and high mass regions. Three new cuts were introduced: the Lepton Veto, the cut on the τ-jet pseudorapidity and the cut on the transverse momentum ratio $\frac{p_T^\tau}{p_t^{\tau top}}$. These new cuts, especially the transverse momentum ratio, allow the lowering of the optimum p_T^τ-cut value, which is particularly important for the low mass region. At the same time, the background rejection for the high mass region could be increased by two to three orders of magnitude compared to cuts used in previous studies, leading to an improvement of the signal-to-background ratio by a factor of at least 25 (low mass region) to more than 100 (high mass region) and to an increase of the significance by a factor of approximately 5-10 for all values of the charged Higgs boson mass.

The jet-tagging was investigated and showed the following results: A τ-tagging efficiency of about 45% maximizes the signal significance. At the same time it leads to a higher signal efficiency, which is crucial for the high mass region where only a few events per year at low luminosity can be expected (depending on $\tan\beta$). Different b-tagging strategies were considered, and it was found that requiring exactly one b-jet with $P_T > 30$ GeV leads to the best performance. Additional requirements for hard b-jets ($|\eta| < 2.0$ & $P_T > 50$ GeV) do not improve the discovery potential.

It was shown that the discovery potential for the charged Higgs boson in the channel $H^\pm \to \tau\nu_\tau$ extends to $m_{H^\pm} = 160$ GeV for all values of $\tan\beta$ with the first three years of LHC data, and up to about $m_{H^\pm} = 170$ GeV in the following years. There is also a significant discovery potential in the region $m_{H^\pm} > m_{top}$ which is currently not covered by any direct searches.

Investigating sources of systematic uncertainties showed a dominating contribution from the τ-tagging uncertainties. Expressed as an error on the statistical significance, the systematic uncertainties lead to a reduction of the significance by about $30 - 60\%$ if the most pessimistic assumptions are applied.

It is expected that additional improvement may be possible by exploiting the τ polarization (see [25]). With the dataset used for this analysis such a cut cannot be investigated due to limitations of the ATLFAST tracking algorithm but in the near future the evaluation of this cut will be possible. A polarization-based cut, together with the various other selection cuts with high discrimination power described in this analysis, constitutes a suitable set of input variables for a multivariate analysis, e.g. via neural networks.

VIII.   ACKNOWLEDGMENTS

APPENDIX A: COMPARISON ATLFAST — FULL SIMULATION

Using ATLAS Full Simulation for the signal and ATLFAST for the background samples in this study raises the question about how well the Fast Simulation (with parametrized detector performance) emulates the Full Simulation of the detector (and the real detector response). In this Appendix we present a comparison of signal performance in Full and Fast Simulation for both the Standard Analysis in Section III and the Improved Analysis in Section IV.

TABLE X: COMPARISON ATLFAST-FULLSIM, STANDARD ANALYSIS: CUMULATIVE SELECTION CUT EFFICIENCY FOR SELECTED MASS POINTS. Standard Analysis cuts as explained in Section III

Cut	$m_{H^\pm} = 200 GeV$		$m_{H^\pm} = 400 GeV$		$m_{H^\pm} = 600 GeV$	
	FULLSIM	ATLFAST	FULLSIM	ATLFAST	FULLSIM	ATLFAST
1 $\tau-$jet	0.243	0.243	0.328	0.335	0.359	0.364
≥ 3 non τ-jets	0.105	0.143	0.155	0.213	0.189	0.251
≥ 1 $b-$jet	0.075	0.088	0.107	0.129	0.133	0.152
≤ 1 hard $b-$jet (a)	0.070	0.082	0.098	0.121	0.122	0.142
W-rec	0.050	0.062	0.067	0.089	0.078	0.102
Top-rec (b)	0.037	0.046	0.048	0.065	0.057	0.071
P_T^τ (c)	0.015	0.016	0.032	0.046	0.047	0.062
P_T^{miss} (d)	0.0061	0.0066	0.023	0.035	0.041	0.055
$\Delta\phi$ (e)	0.0025	0.0024	0.0213	0.0321	0.0391	0.0525

TABLE XI: COMPARISON ATLFAST-FULLSIM, STANDARD ANALYSIS: RELATIVE SELECTION CUT EFFICIENCY FOR SELECTED MASS POINTS. Standard Analysis cuts as explained in Section III

Cut	$m_{H^\pm} = 200 GeV$		$m_{H^\pm} = 400 GeV$		$m_{H^\pm} = 600 GeV$	
	FULLSIM	ATLFAST	FULLSIM	ATLFAST	FULLSIM	ATLFAST
1 $\tau-$jet	0.24	0.24	0.33	0.34	0.36	0.36
≥ 3 non τ-jets	0.43	0.59	0.47	0.64	0.53	0.69
≥ 1 $b-$jet	0.72	0.61	0.69	0.60	0.70	0.61
≤ 1 hard $b-$jet (a)	0.67	0.57	0.63	0.57	0.65	0.57
W-rec	0.72	0.76	0.68	0.74	0.64	0.72
Top-rec (b)	0.73	0.75	0.72	0.73	0.73	0.70
P_T^τ (c)	0.41	0.35	0.67	0.70	0.81	0.86
P_T^{miss} (d)	0.40	0.40	0.72	0.77	0.89	0.89
$\Delta\phi$ (e)	0.41	0.37	0.92	0.91	0.95	0.95

For the Standard Analysis, Tables X and XI compare the Fast and Full Simulation cumulative and relative efficiencies, respectively, for $m_{H^\pm} = 200, 400$ and 600 GeV. The last row of Table X shows that the ATLFAST efficiencies are significantly higher with the exception of the events with $m_{H^\pm} = 200$ GeV. This difference between ATLFAST and Full Simulation results can be understood from the difference in the observed jet-multiplicity between the two simulation techniques. ATLFAST is known for overestimating the jet reconstruction efficiency at low P_T thus giving rise to significantly more jets in the region up

to about 50 GeV [26]. Figures 31 and 32 show the multiplicities for light jets and b-Jets. The number of events with at least three reconstructed parton jets is significantly higher for ATLFAST. The b-Jet performance is comparable for ATLFAST and Full Simulation. The impact of the difference can be seen on the relative efficiencies for each cut (Table XI) where in ATLFAST the efficiency is much higher for passing the cut on having 3 or more non-τ jets. Since a large fraction of jets from a W decay is below 40 GeV there is also an impact on passing the cut on W reconstruction since in ATLFAST more of the real W-jets are reconstructed.
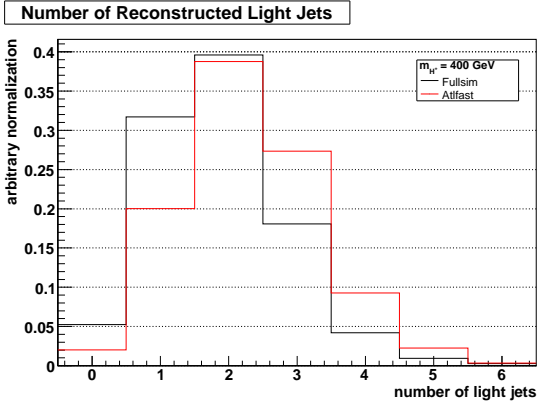

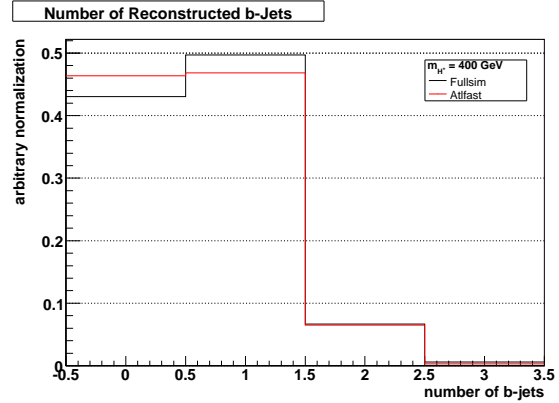FIG. 31: NUMBER OF RECONSTRUCTED LIGHT JETS WITH $p_T > 30$ GEV

FIG. 32: NUMBER OF RECONSTRUCTED b-JETS WITH $p_T > 30$ GEV

Having pointed out the differences between Full Simulation and ATLFAST it is worth pointing out that also some excellent agreements can be observed. Tables X and XI show that the reconstruction and tagging of τ-jets and the p_T^{miss} reconstruction match very well between the two simulation techniques: Figures 33 and 34 show that the differences observed between Full Simulation and ATLFAST are small. W boson and top quark reconstruction also compares well as can be seen in Figures 35 and 36, except for a known jet energy miscalibration in Full Simulation in the software release used in this study.

A comparison of the selection cut flow between Full Simulation and ATLFAST for the Improved Analysis is shown in Tables XII and XIII. The total selection cut efficiency here is more similiar. The reason is the new p_T Ratio cut which is a cut on the ratio between p_T^τ and the p_T of the hardest parton jet in the event which was not used for reconstructing the top quark. The jet multiplicity in ATLFAST events is higher and thus the p_T Ratio cut has a smaller efficiency when the signal is simulated with ATLFAST as compared to Full Simulation. This compensates the ATLFAST efficiency increase for the cuts on at least three reconstructed parton jets, and on the W and top quark reconstruction which is also caused by the higher jet multiplicity.

This investigation shows that in spite of some discrepancies, Full and Fast Simulation lead to similar overall results for the signal efficiency since the ATLFAST jet multiplicity overestimation has opposite effects on two selection cuts. This helps to draw conclusions about how appropriately the main background channel, $t\bar{t}$, is described in ATLFAST, and how this affects the results of applying the selection cut chain presented in this study:

- Requirement of at least three parton jets: Even for a more realistic jet reconstruction efficiency than the one in ATLFAST, a $t\bar{t}$ efficiency close to one and thus no difference between Full and Fast Simulation is expected for this selection cut.

- W and top quark reconstruction: Because of their similar nature it is expected that the ATLFAST

efficiency overestimation of these cuts is comparable for signal and $t\bar{t}$ background.

- p_T Ratio: The additional ATLFAST jets lead to an underestimation of the efficiency of this cut, however, this effect is expected to be smaller for the $t\bar{t}$ background since there are anyway additional jets from the hard process in the event which are in average hard enough not to be affected by the ATLFAST jet reconstruction efficiency overestimation. The initial and final state radiation jets which cause the discrepancy of the signal efficiency of this cut between Full and Fast Simulation are in average much softer and thus do not enter into the calculation of the p_T Ratio for the $t\bar{t}$ background.

This leads to the conclusion that the results obtained by comparing Full Simulation signal to Fast Simulation background are conservative. It is expected that the $t\bar{t}$ rejection is underestimated by approximately 10% ($t\bar{t}$ is close to the low mass signal considering the transverse momenta involved, but close to the high mass signal considering the jet activity), as observed for the signal, but potentially higher for the reasons stated above. This, however, has to be confirmed by future studies using Full Simulation for $t\bar{t}$.
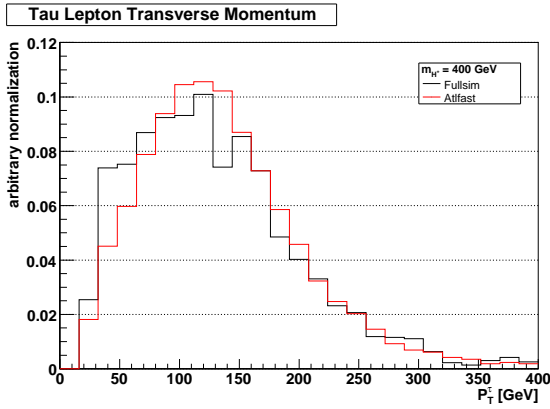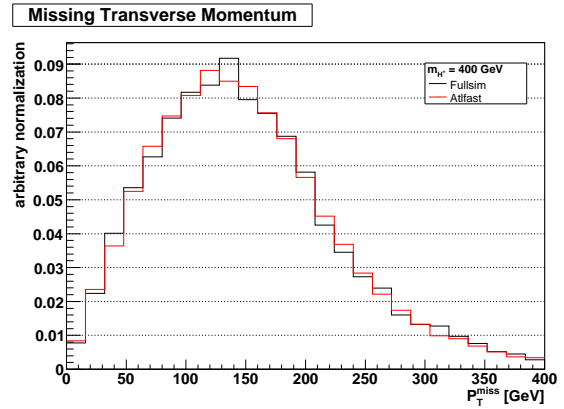
FIG. 33: TAU-JET TRANSVERSE MOMENTUM

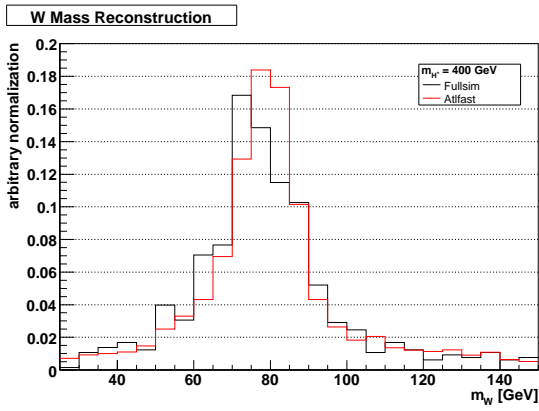FIG. 34: MISSING TRANSVERSE ENERGY
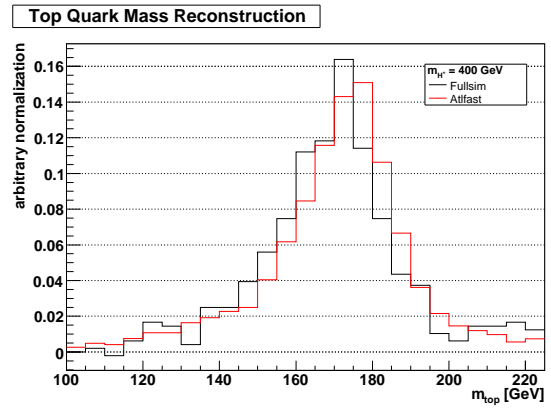
FIG. 35: W BOSON RECONSTRUCTION

FIG. 36: TOP QUARK RECONSTRUCTION

TABLE XII: Comparison Atlfast-Fullsim, Improved Analysis: Cumulative Selection Cut Efficiency for Selected Mass Points. Improved Analysis cuts as explained in Section IV

Cut		$m_{H^\pm} = 200GeV$		$m_{H^\pm} = 400GeV$		$m_{H^\pm} = 600GeV$	
		FullSim	Atlfast	FullSim	Atlfast	FullSim	Atlfast
1 $\tau-$jet		0.243	0.243	0.328	0.335	0.359	0.364
≥ 3 non τ-jets		0.105	0.143	0.155	0.213	0.189	0.251
1 $b-$jet		0.057	0.073	0.083	0.108	0.103	0.126
Lepton veto	(a)	0.056	0.073	0.082	0.107	0.102	0.125
W-rec		0.042	0.055	0.055	0.078	0.066	0.088
Top-rec	(b)	0.032	0.041	0.040	0.057	0.048	0.061
$|\eta_\tau|$		0.018	0.024	0.025	0.035	0.034	0.045
Ptratio		0.016	0.018	0.017	0.022	0.025	0.030
P_T^τ	(c)	0.0082	0.0099	0.0141	0.0191	0.0227	0.0276
P_T^{miss}	(d)	0.0023	0.0023	0.0091	0.0114	0.0160	0.0194
$\Delta\phi$	(e)	0.0009	0.0007	0.0082	0.0099	0.0154	0.0188

TABLE XIII: Comparison Atlfast-Fullsim, Improved Analysis: Relative Selection Cut Efficiency for Selected Mass Points. Improved Analysis cuts as explained in Section IV

Cut		$m_{H^\pm} = 200GeV$		$m_{H^\pm} = 400GeV$		$m_{H^\pm} = 600GeV$	
		FullSim	Atlfast	FullSim	Atlfast	FullSim	Atlfast
1 $\tau-$jet		0.24	0.24	0.33	0.34	0.36	0.36
≥ 3 non τ-jets		0.43	0.59	0.47	0.64	0.53	0.69
1 $b-$jet		0.54	0.51	0.54	0.50	0.54	0.50
Lepton veto	(a)	0.98	1.00	0.98	0.99	0.99	0.99
W-rec		0.76	0.75	0.67	0.73	0.65	0.70
Top-rec	(b)	0.74	0.75	0.74	0.73	0.73	0.70
$|\eta_\tau|$		0.58	0.59	0.62	0.61	0.70	0.74
Ptratio		0.85	0.72	0.69	0.63	0.73	0.67
P_T^τ	(c)	0.53	0.56	0.82	0.87	0.92	0.92
P_T^{miss}	(d)	0.28	0.24	0.65	0.60	0.70	0.70
$\Delta\phi$	(e)	0.39	0.29	0.90	0.87	0.96	0.97

[1] Richter-Was E., Froidevaux, D., Poggioloi, L., *ATLFAST 2.0: A Fast Simulation Package for ATLAS*. Atlas Internal note, ATL-PHYS-98-131, Cern: Geneva (1998)

[2] Assamagan, K., Coadou, Y., *Prospects for the Determination of the Charged Higgs Mass and* $\tan\beta$ *with the* Atlas *Detector at the Large Hadron Collider*. Acta Physica Polonica B 33 (2002) 1347-1360

[3] Alwall, J., Rathsman, J., *Improved Description of Charged Higgs Boson Production at Hadron Colliders*. JHEP12 (2004) 050

[4] Alwall, J., *MATCHIG: A program for matching charged Higgs boson production at hadron colliders*. (2005) hep-ph/0503124

[5] Assamagan, K., Coadou, Y., *The Hadronic* τ *Decay of a Heavy* $H^{\pm}$ *in ATLAS*. Acta Physica Polonica B 33 (2002) 707-720

[6] Plehn, T., *Higgs-Boson Production Induced by Bottom Quarks*. Phys.Rev. D69 (2004) 094005

[7] Plehn, T., *Charged Higgs Boson Production in Bottom-Gluon Fusion*. Phys. Rev. D67 (2003) 014018

[8] Beneke, M. and others, *Top quark physics*. (2000) hep-ph/0003033

[9] Gunion, J.F., Haber, H.E., Kane, G., Dawson, S., *The Higgs Hunter's Guide*. Perseus Publishing: Cambridge, Massachussetts (1990)

[10] Sjostrand, Torbjorn and Lonnblad, Leif and Mrenna, Stephen, *PYTHIA 6.2 Physics and Manual*. (2001) hep-ph/0108264

[11] Was, Z., Golonka, P., *TAUOLA as tau Monte Carlo for future applications*. Nucl. Phys. Proc. Suppl. 144 (2005) 88-94

[12] Barberio, E., Was, Z.,*PHOTOS- a universal Monte Carlo for QED radiative corrections: version 2.0*. Comp. Phys. Commun. 79 (1994) 291

[13] Heldmann, M., Cavalli, D., *An Improved* τ*-Identification for the ATLAS Experiment*. Atlas Internal Note, ATL-PHYS-PUB-2006-008, Cern: Geneva (2006)

[14] Correard, S., et al., *b-tagging with DC1 data* Atlas Internal note, ATL-PHYS-2004-006

[15] Mangano M. L., Moretti M., Piccinini F., Pittau R. and Polosa A., *ALPGEN, a generator for hard multiparton processes in hadronic collisions*, JHEP 0307:001,2003, hep-ph/0206293.

[16] Susy Group (online): https://twiki.cern.ch/twiki/bin/view/Atlas/AtlFastProduction

[17] Slabospitsky, S. R., Sonnenschein, L., *TopRex Generator (version 3.25). Short Manual*, Comput. Phys. Commun. 148 (2002) 87-102

[18] Cavalli D., Resconi S., *Combined Analysis of* $A \to \tau\tau$ *Events from Direct and Associated* $b\bar{b}A$ *Production*. Atlas Internal Note, ATL-COM-PHYS-99-010

[19] EventView (online): https://uimon.cern.ch/twiki/bin/view/Atlas/EventView

[20] Brun, R., Rademakers, F., *ROOT - An Object Oriented Data Analysis Framework*. Nucl. Inst. & Meth. in Phys. Res. A 389 (1997) 81-86

[21] Biscarat, C., Dosil, M., *Charged Higgs search in top quark decays with the ATLAS detector*. Atlas Internal Note, ATL-PHYS-2003-038

[22] Gianotti, F., *Precision Physics at LHC*. Atlas Internal Note, ATL-PHYS-99-001

[23] Atlas Collaboration, *ATLAS Detector and Physics Performance Technical Design Report*. Volume 1, Cern: Geneva (1999)

[24] Buescher V., et al. *Tevatron-for-LHC Report: Preparations for Discoveries*. (2006) hep-ph/0608322

[25] Raychaudhuri, S., *Sharpening up the Charged Higgs Boson Signature using Tau Polarization at LHC*. Phys. Rev. D53 (1996) 4902-4908

[26] Cavalli, D., et al., *Performance of the ATLAS fast simulation ATLFAST*. ATL-COM-PHYS-2007-012